UNIVERSITY OF COPENHAGEN

Novel nanophotonic interface for droplet GaAs quantum dots

Hanna Salamon

Under supervision of Prof. Peter Lodahl and Dr. Alexey Tiranov

Niels Bohr Institute

University of Copenhagen

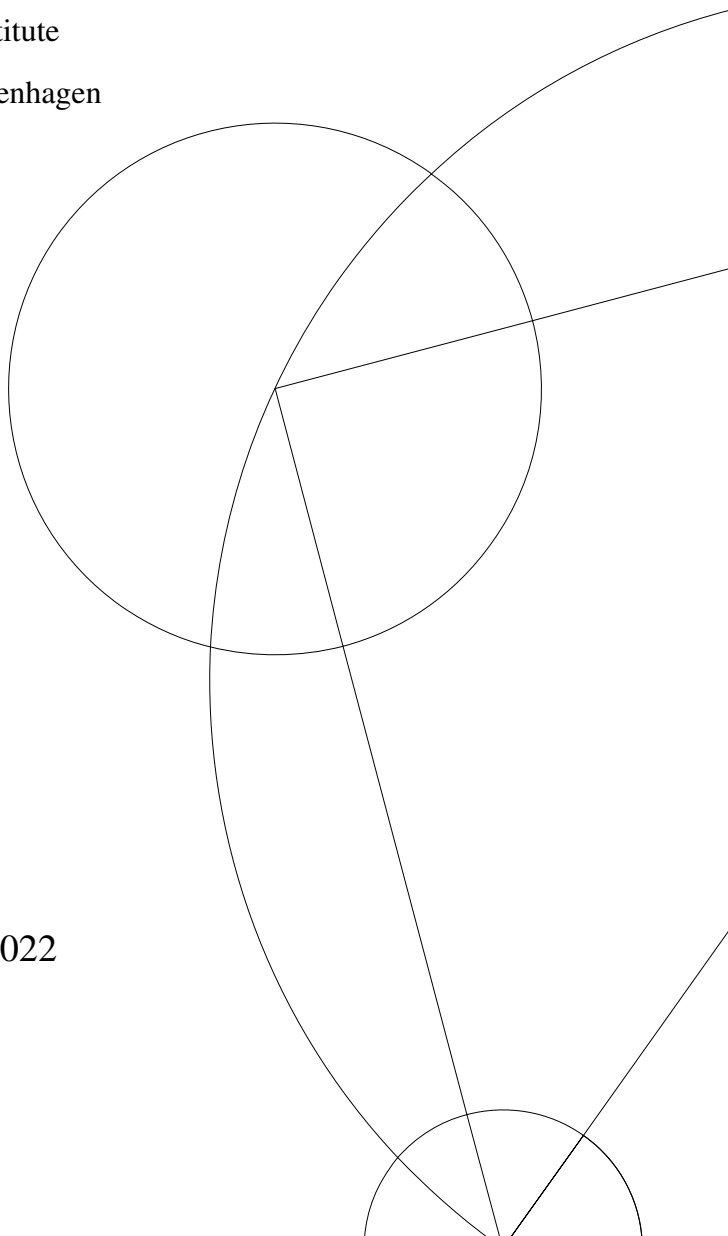

November 2022

ABSTRACT

GaAs quantum dots (QDs) are nanostructures embedded in a AlGaAs host material which can be fabricated via droplet epitaxy. A low Al concentration of the host material is a critical requirement for the quality of GaAs QDs as a single photon source (SPS) for quantum optics and photonic devices for scalable quantum networks. However, the reduction of the Al concentration has a been a challenge limiting the quality and thereby the potential of GaAs as SPSs for photonic quantum devices.
Recently, advancements in the fabrication of droplet GaAs QDs allowed for a drastic reduction of the Al concentration and thus introducing a novel generation of QDs. Droplet GaAs QDs have proven to be (i) reliable in fabrication, (ii) SPSs of outstanding quality, and (iii) are emitting in the spectral range of the Rubidium D-1 and D-2 lines. This new generation of GaAs droplet QDs thus promises to leverage the progress towards large scale production of photonic devices for scalable quantum networks. In particular, the compatibility with rubidium based quantum memories allows for quantum information processing applications.
The main goal of the project is to design and characterize photonic circuits based the new generation GaAs droplet QDs as embedded SPSs. More specially, the target is to realize light-matter interfaces of GaAs droplet QDs and nanophotonic waveguides. The nanophotonic waveguides will be tailored to enhance and modify light-matter interfaces for deterministic coupling, high purity and bright single photon emission. DC-stark tuning and charge tuning will be demonstrated by embedding the nanophotonic devices in a n-i-p diode. The properties of the light-matter interface will be investigated experimentally using high-resolution and time-resolved optical spectroscopy. Specifically, the purity and the efficiency of the SPS will be determined.

ACKNOWLEDGEMENTS

First of all I would like to thank Nils Valentin Hauff with whom I have spent the past year together in the lab. Thank You for all the help, support and for all the friendly conversations about climbing. I would also like to thank my supervisors, Alexey Tiranov for helping me with writing this thesis and the support in the lab and Professor Peter Lodahl for giving me an opportunity to work in the Quantum Photonics group. I also want to thank all the members of HyQ lab for creating a very friendly and welcoming atmosphere. Finally, I would like to thank my brother Tymoteusz Salamon for supporting me on every stage of my education and for all valuable advice.

CONTENTS

1

INTRODUCTION

In the recent decades we have been witnessing a technological revolution starting from the first prototype of a classical computer up until now when the internet is accessible from everyone's smartphone and literally all possible information is right at our fingertips. There are however limitations to classical internet among others the speed of data transfer, but what is more important is how easy eavesdroppers can access the transmitted information. Nowadays scientists are on the verge of applying a quantum effects to provide a secure technology. It is believed that quantum internet will begin a new technological revolution, however the implementation and a commercial application are very challenging [1].

The classical internet is based on the bits of light, where the information is coded as 1 ("on") or 0 ("off"). The quantum internet is using the same logic, however the information is coded in quantum bits (qubits). The qubits are represented by the single photon states $|0\rangle$ and $|1\rangle$. Due to the unique properties of qubits such as superposition, entanglement, and teleportation, it gives an advantage over the classical network in many aspects.

A quantum internet requires a quantum communication to protect information channels against eavesdropping using quantum cryptography. The most well known protocol of quantum cryptography is the so-called quantum key distribution (QKD), e.g. the BB84 [2] protocol, which uses single photon polarization to write a random sequence of "0" and "1" numbers used as a cryptographic key in the actual communication. In the safe quantum channel, a quantum key is generated and transmitted, while the classical channel transmits information to the receiver on selected bases in which the photon polarization is measured. In a secure quantum channel it is checked whether the eavesdropper tried to extract information on the qubits stream. A third party trying to eavesdrop on the key has to perform a measurement, which introduces a detectable disturbance to the system.

The realization of quantum communication protocols like BB84 requires deterministic on-demand single photon emitter: the quantum light source that provides single photons.

There are several known methods to generate single photons i.a. spontaneous parametric down conversion (SPDC) [3,4], defects in carbon nanotubes [5], ion trapping [6] using defects in semiconductors [7] and the use of optical transitions within semiconductor quantum dots (QDs).

It has been already shown that semiconductor QDs are suitable candidates for deterministic and practical high-quality single photon source (SPS) [8,9] as they are a good approximation of a two-level system which emits only one single photon at a time. Additionally, epitaxially grown semiconductor QDs allow site control during growth [10] and can be fabricated inside optical cavities or photonic

structures for emission enhancement and control [11,12]. By applying electric or magnetic field the energy structure of a QD can be modified which also enable a fine tuning of emission energy.
Ideally SPS should be compatible with telecom spectral range around 1.55 µm (telecom C-band window) for long distance quantum communication due to compatibility with existing silica fiber networks [13]. Most of the QD-based devices has been mainly demonstrated in the visible and near infrared range [14,15]. Up till now QDs based on InGaAs grown in the Stranski–Krastanov- mode in a GaAs matrix have been studied the most. These QDs show excellent electronic and optical properties for quantum applications [16], but their emission wavelength range is again limited to around 1300 nm. For the development of QD-based quantum photonics it is important to extend the wavelength range towards shorter and longer wavelengths.
Recently GaAs QDs have gained a lot of interest due to novel fabrication method which is based on local droplet etching and provide a low Al concentration of the host material which is crucial requirement for the quality of GaAs QDs and their potential application as a SPS [17]. Embedding these nanostructures into n-i-p diode specially designed for low-temperature operation has proven an ultra-low noise behavior. The charge control possible via Coulomb blockade has significantly reduced the charge noise improving close-to lifetime-limited linewidths and showing no blinking [18].
Droplet GaAs QDs are emitting light in the range of 700- 800 nm which potentially enables the storage of QD single-photons in a quantum memory made of a rubidium atoms ensemble [19] and also spectrally overlap with the highest efficiency of silicon detectors [20]. Additionally, droplet GaAs QDs have typically more symmetric shapes, facilitating the creation of polarisation-entangled photon pairs from the biexciton cascade [21] which can be used for quantum information applications among others to realize quantum teleportation, implement quantum logic and computation operations [22]. Since the fabrication of GaAs QDs is based on the local droplet etching the QDs are formed deterministically and are characterized by low levels of strain in contrast to well-known InGaAs QDs which are fabricated via strain mismatch of neighboring materials [23].
The main goal of the master thesis was to experimentally investigate the optical properties of a GaAs QDs in AlGaAs host material embedded in a nanophotonic devices (based on photonic crystal waveguide (PhCW), nanobeam waveguide (NB) and shallow etched grating (SEG).
The motivation of conducted research was to investigate droplet GaAs QDs in a nanophotonic devices with simultaneous charge control, which has not been demonstrated yet.
When a QD is efficiently coupled to a PhCW, emitted photons are transferred directly to the propagating single mode of a PhCW which enable a deterministic and coherent operation of a photon source [24]. Furthermore, when a quantum emitter is embedded in a PhCW an enhanced light- matter interaction is expected due to Purcell effect [25], which allows to shorten the lifetime of the carrier and, as a result, increases the spontaneous emission rate from the QD. Since the PhCW is not limited to a narrow spectral bandwidth as in an optical cavity (where the bandwidth is determined by a high quality factor (Q factor) of a cavity), a precise control of a QD position is not needed [26]. Instead, photons are emitted with large probability to the localized mode of the cavity at a strongly enhanced rate.
It has been shown that quantum emitters in PhCW are characterized by high- efficiency and high purity,

which makes them a great candidate for on-chip quantum information processing and computing [27,28]. The integration of QDs with various photonic elements, compatibility with electronic systems and the possibility of scaling such a device will allow for wider applications in the field of quantum information processing, as well as for the commercialization and popularization of the device. The nanophotonic devices however, still suffer from the surface roughness, displacements, vacancies and other unavoidable fabrication imperfections which generate high propagation losses in the waveguides in an order of over a dozen dB / mm [29].

All the measurements were performed in a high- resolution optical setup adjusted for excitation from two ports (out-of plane and through the SEG). The QD emission is reflected on SEG (specially design trenches) and collected into a fiber. As part of a project a filtering setup based on a transmission grating was designed and built. It enables the laser filtering and therefore a detection using highly sensitive APD detectors. The basic characterization of the grating filter filter was performed.

As part of the research for the master thesis, a bright single QD in a PhCW was characterized in two different temperatures (in XK- a temperature between 15- 20K and at cryogenic 7K). For most measurements QD was excited quasi- resonantly. A dependence of the applied bias voltage on the QD emission was measured which enabled to estimate the Stark shift. The emission line of a QD was measured for several different excitation powers in order to identify the exciton state. Moreover, a linewidth of a QD emission was determined and compared for both temperatures. A single photon purity of a quantum emitter was obtained from a Hanbury Brown and Twiss experiment. A bandwidth of a quasi-resonant excitation as well as resonance fluorescence were determined and compared. The difference in the bandwidth for both temperatures enabled to identify the temperature of the sample. Conducted research as part of a master thesis gave an insight into a novel photonic device based on GaAs QD SPS in a n-i-p diode embedded in a PhCW.

Performed measurements represent the first approach in characterization of GaAs QDs in nanophotonic devices which might have a wide application in a quantum information and quantum computing. The obtained results are needed for the implementation of the next generation of more complex photonic integrated systems based on GaAs QD SPS which in the future could be used in realization of a quantum repeaters based on rubidium quantum memories.

2

INTRODUCTION TO QUANTUM DOTS

Semiconductor QDs are being extensively researched for the development of solid state single photon emitters, which are required for optical quantum computing and related technologies such as quantum key distribution and quantum metrology. In this chapter the unique properties of these quantum emitters as well as the basic operational principles and the physics behind is presented.

2.1 ENERGY STRUCTURE, QUANTUM SIZE EFFECT AND DENSITY OF STATES

Low-dimensional semiconductor structures, due to the specific energy structure are widely used in optoelectronics, electronics and nanophotonics [30,31,32]. Especially QDs - zero-dimensional structures with dimensions in the order of nanometers attract more and more interest [33]. With such small size the so-called quantum confinement effect appears. In QDs the movement of carriers is spatially limited in all three dimensions, which causes quantization of energy in each direction - the appearance of discrete energy levels. The presence of discrete energy states translates into the form of the electron density of states $\rho(E)$, which is defined as the ratio of the number of states per unit of energy [34]:

$$\rho(E) = \frac{dn(E)}{dE}, \tag{1}$$

where n is the number of available energy states, and E - energy. In QDs, the density of states function takes the form of the sum of the Dirac delta function (Fig. 1), which means that carriers can only occupy energy levels with strictly defined energies, just like in an atom.

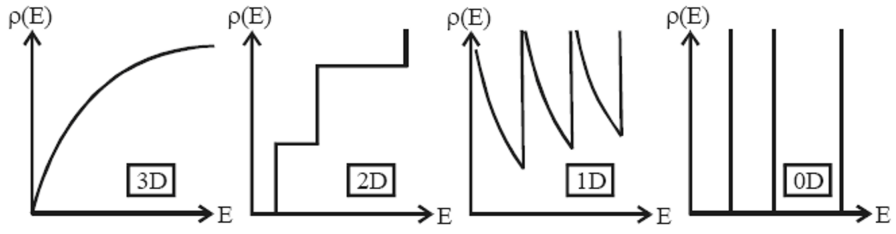

Figure 1: The dependence of the density of states function on the energy of carriers for structures of different dimensions [35].

The diagram above shows the dependence of the density of states on the energy of carriers for low-dimensional structures. For a bulk material, the dependence of the density of states on energy is smooth and increase monotonically proportionally to $E^{1/2}$, for a structure limited in one dimension (e.g. a quantum well) this relationship is stepped, for a structure limited in two dimensions (e.g. a quantum wire) the function is partially continuous, while for zero-dimensional structures - QDs, the density of states function is discrete.

Additionally, in low-dimensional structures we can observe a quantum size effect [36]. The quantum size effect describes the dependence of the energy structure on the size of the object (Eq. 2) and it is the most convenient to describe using the example of a quantum well. Quantum well is fabricated by having a material sandwiched between two layers of a material with a wider band gap (Fig. 2).

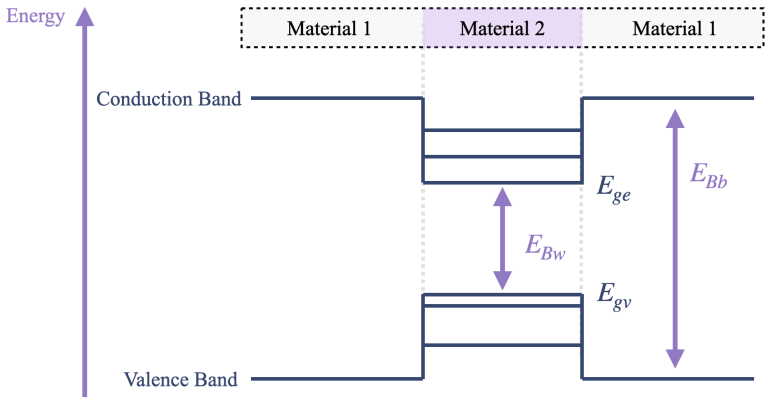

Figure 2: Scheme of a single quantum well, where E_{Bw} is a band gap of a well material and E_{Bb} is the band gap of a barrier. The E_{ge} and E_{gv} denote the ground state of the conduction and valence band respectively.

To a good approximation we can consider that the potential well has an infinite depth since the depth of the bonding potential is significantly greater than the thermal energy of the carriers at room temperature (or at low temperature - if we study its behavior under such conditions). For an infinite one-dimensional potential well, the size effect can be solved analytically. If the width of a quantum well is comparable to the de Broglie wavelength of the electron, the quantization of energy in that direction takes place, and the energy of subsequent energy states is expressed by [37]:

$$E_z = \frac{n_z^2 \hbar^2 \pi^2}{2mL^2}, \tag{2}$$

where n_z is a natural number of consecutive energy levels, $\hbar$ - Dirac constant, m is the mass of the carrier, and L is the width of the well.

The above formula shows that as the width of the quantum well increases, the energy of individual energy states decreases and the effective band gap increases (the distance between the ground states in both bands) (Fig. 2). Depending on the carrier - electron or hole, the energy of the levels will have a different value in the conduction band (the band of electron orbitals in which electrons can jump up into from the valence band when excited) and in the valence band (the band of electron orbitals in which electrons can jump out to the conduction band when excited), due to different effective masses-

a mass of carrier that interacts with the material environment. For a QD, we must take into account that the quantization of energy takes place in all three dimensions, therefore the formula describing the energies of states (1) has to be modified accordingly:

$$E_{x,y,z} = \frac{\hbar^2 \pi^2}{2m} \left(\frac{n_x^2}{L_x^2} + \frac{n_y^2}{L_y^2} + \frac{n_z^2}{L_z^2} \right), \tag{3}$$

where n_x, n_y, n_z denote respectively the numbering of states in the direction x, y, z. The energy structure of a QD can be modified by applying an external electric field via Stark Shift which enable a fine tuning of emission energy. The tuning range depends on the growth and can be optimized and to some degree regulated [38].
Accordingly, the emission wavelength can be also modified by applying magnetic field via Zeeman shift [39] or by a temperature tuning [40] and a stress tuning [41].

2.2 EXCITONIC STATES

During the absorption of energy by the semiconductor material, an electron can be excited from the valence band to the conduction band, thereby leaving one unoccupied state in the valence band- a hole. The spatial location of charge carriers in low- dimensional structures brings the Coulombic interaction of the generated electron-hole pair creating a bound state called exciton- a new quasiparticle defined as an interacting pair of charge carriers of the opposite sign. Such defined exciton (X) is electrically neutral (it is not a charge carrier) and only transfers energy [42]. Depending on the distribution of carriers, other exciton states may occur in a QD (Fig. 3). An example is biexciton (XX) – a four – particle state, which consists of two electrons and two holes (two excitons)- it is electrically neutral. We also distinguish charged states (with an odd number of carriers) - positively charged excitons (X^+) and negatively charged (X^-) excitons, the so-called trions. A positive trion consists of one electron and two holes, and a negative trion consists of two electrons and one hole.

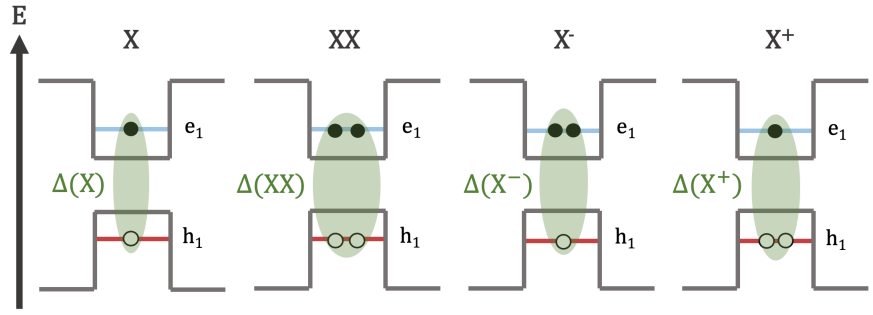

Figure 3: Diagram of single-particle states building basic exciton states in the ground state, X - exciton, XX - biexciton, X^- - negative trion, X^+ - positive trion; e_1 is the lowest electron state in the conduction band and h_1 is the ground state of the hole in the valence band. The binding energies of the individual excitonic states are marked with green.

The strength of interaction between carriers in excitonic states is referred as the binding energy. It is defined as the difference of the sum of the energies of the free particles and the energy of the bound

complex E.
For individual states, it is described by the equations:

$$\Delta(X) = (\epsilon_0^e - \epsilon_0^h) - E(X),$$
$$\Delta(X^-) = (\epsilon_0^e + E(X)) - E(X^-),$$
$$\Delta(X^+) = (-\epsilon_0^h + E(X)) - E(X^+),$$
$$\Delta(XX) = 2E(X) - E(XX),$$

where Δ is the binding energy, while ϵ_0^e and ϵ_0^h are the energy of the free electron and the hole that does not interact with it, respectively. The binding energy of biexciton is lower than the exciton recombination energy, due to the Columb force between the two electrons.
Radiative recombination of any exciton state results in the emission of a photon which energy corresponds to the energy difference between the individual energy levels (considering the binding energy).

2.3 DYNAMICS OF CARRIERS

The probability of an optical transition per unit time between two states (initial $|i\rangle$ and final $|j\rangle$) Γ_{ij} in a QD is described by the Fermi Golden Rule [43]. Its inverse is the time of radiative recombination from a given state:

$$\tau_{i-j} = \frac{1}{\Gamma_{ij}}. \tag{4}$$

The time of radiative recombination can be modified e.g. by placing the emitter in the optical cavity [29] or in the photonic structures [26].
The probability to occupy a given state depends on the excitation power, temperature as well as relaxation of carriers between states. The decay of the excitation is described using a model of kinetic equations. The solutions of kinetic equations allow to determine the dependence of the intensity of the emission from a given exciton state on time (in the case of pulsed excitation) or the rate of generation of carriers in the QD depending on the excitation power density. This model allows the identification of individual lines in the emission spectrum from a QD and assigning them to specific excitonic states using the dependence of emission intensity as a function of excitation power.
In the simplest case, when only three states in the system are considered: ground state - 0 (no carriers in the QD), exciton - X and biexciton – XX, kinetic equations, assuming that only transitions between neighboring states are possible, take the following form:

$$\frac{dp_x}{dt} = gp_0 + \frac{p_{xx}}{\tau_{xx}} - \frac{p_x}{\tau_x} - gp_x, \tag{5}$$
$$\frac{dp_{xx}}{dt} = gp_x - \frac{p_{xx}}{\tau_{xx}}, \tag{6}$$

where p_0, p_x and p_{xx} are respectively the probability of no exciton in a QD, one exciton and biexciton (in the absence of other states: $p_0 + p_x + p_{xx} = 1$), while g is the generation rate, which is directly proportional to the excitation power density, τ_x and τ_{xx} are the lifetime of the exciton and biexciton. The intensity of emission from a given state is directly proportional to the probability of its occupation and the rate of recombination of carriers, therefore expressions describing the intensity of exciton emissionI_x and I_{xx} can be written as:

$$I_x \sim \frac{p_x}{\tau_x} = \frac{g}{1 + g\tau_x + g^2\tau_x\tau_{xx}} \sim P, \tag{7}$$

$$I_{xx} \sim \frac{p_{xx}}{\tau_{xx}} = \frac{g^2\tau_x}{1 + g\tau_x + g^2\tau_x\tau_{xx}} \sim P^2, \tag{8}$$

where P denote excitation power density. Therefore, it is possible to distinguish the emission from exciton and biexciton. In the range of low excitation powers, the dependence of the emission intensity on the excitation power is linear for exciton and quadratic for biexciton.

2.4 CHARGE ENVIRONMENT

Control and understanding of charge states in a QD is important for applications in quantum information processing or quantum communication. In QDs due to semiconductor environment a random additional charge can occur e.g., due to impurities in the material, by scattering an electron from the wetting layer, or the bulk material into the QD or due to surface states. Whenever an electron enters the QD, its emission is shifted in a process called spectral diffusion, effectively increasing the linewidth of QD emission. The charge noise can lead to many problems mainly blinking and the optical linewidths well above the transform limit [44,45]. It has been proven that embedding InGaAs QDs in a n-i-p structure can improve significantly the performance of the devices i.a. the charge state can be locked by Coulomb Blockade [46,47], the significant reduction of charge noise is possible [48] and the exact transition frequency can be tuned in-situ via a gate voltage [49].
In order to apply an external electric field on a QD structure the emitter needs to be placed in the center of a diode structure (for example between a n-type semiconductor and a p-type semiconductor region making a n-i-p diode structure, like mentioned before InGaAs QDs) (Fig. 4). The charge carriers are moving from p and n layers, allowing the current flow through the membrane with QDs. To allow the current flow through the structure, the sample needs to have a special metal contacts deposited on the p and n layer.

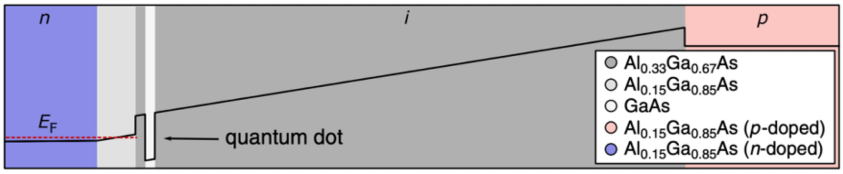

Figure 4: Schematic band structure (conduction band) of the diode hosting charge-tunable GaAs QDs. Figure adapted from [17].

The Fermi level (E_F) of the diode structure is defined by the electron-rich n layer. The i region between the QD layer and the n-doped layer forms a barrier between the quantum well and the reservoir of electrons.
The conduction and valence bands are bent due to the built in and the high tunnel barrier is preventing electrons to enter the QD. When applying a voltage, conduction and valence bands are bent towards the flat band configuration until the diode opens and charge carriers flow through the diode and the exciton in a QD can be trapped.
Moreover, an applied external electric field allows a fine tuning of the emission energy from the emitter via Stark Shift. Tuning the QD emission allows to change the emission energy such that it can be in resonance with the optical cavity, laser or a different QD. External electric field enables to "switch on" and "switch off' the QD emission, which gives a quick and reliable background measurement.

2.5 QUANTUM DOT AS A SINGLE PHOTON SOURCE

It has already been demonstrated that QDs are suitable candidates for deterministic and practical high-quality single photon sources (SPSs) [8,9] since they are a good approximation of a two-level system which inherently emits single photons. SPSs based on spontaneous emission in a single QD provide several advantages compared to other sources: they are photostable, compatible with chip technology, have a short lifetime together with a lifetime limited emission line at low temperature, are available over a broad spectral range from the near-infrared to UV, and allow to produce entangled multiphoton states via cascaded decay of higher excitations [50, 51, 52]. The ideal SPS needs to have high purity (the single-photon purity is quantified by the measured degree of second-order coherence function $g^{(2)}(\tau)$ and should emit indistinguishable photons (verified using Hong–Ou–Mandel experiment) with a long coherence time (coherence length of a light source is determined by its ability to emit photons of similar wavelength and phase). The purity of the source can be quantified through the second order correlation function $g^{(2)}(\tau)$:

$$g^{(2)}(t,\tau) = \frac{\langle a^{\dagger}(t)a^{\dagger}(t+\tau)a(t+\tau)a(t)\rangle}{\langle a^{\dagger}(t)a(t)\rangle^2}, \tag{9}$$

where $a(t)$ and $a^{\dagger}(t)$ are the field annihilation and creation operators at time t and delay τ. The function can be best understood in the respect to the Hanbury Brown and Twiss (HBT) experiment (Fig. 5) [53]. The experiment is based on the interferometer which measure the correlation in intensities. For an ideal SPS $g^{(2)}(\tau = 0)) = 0$, meaning that two photons are never in the two detectors at the same time. The measurement of a $g^{(2)}(0))$ function of a SPSs can be still limited by the background light that enter into the experiment and give a false two photon detection or simply by imperfections of the source itself. So far a $g^{(2)}(0)$ as low as $9.4x10^{-5}$ was reported using two- photon excitation on GaAs/AlGaAs QDs [54].
After the emission of a photon a single emitter can be re-excited (and emit a second photon) only

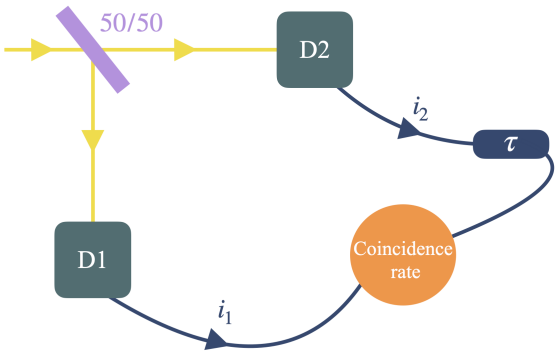

Figure 5: Hanbury Brown and Twiss experiment setup. Beam of photons split on 50/50 beam splitter and are detected on each path with single photon detectors. Detection events are analyzed by measuring coincidences between two detectors.

when it has returned from the excited state. Therefore, the emission of a several photons in an ideal two-level system is not possible as the time between emitting photons is limited by excited-state lifetime. This is so-called anti-bunching and leads to $g^{(2)}(\tau = 0) = 0$. Anti-bunching can also refer to sub-Poissonian photon statistics, that is a photon number distribution for which the variance is less than the mean [55].

2.6 SPONTANEOUS EMISSION OF A TWO LEVEL SYSTEM

The control of spontaneous emission of a QD is necessary for diverse applications i.a. a SPS for quantum information [56]. One of the platforms to control the spontaneous emission of an emitter is via vacuum fluctuation of a dielectric environment. An example is embedding a QD into a nanophotonic devices which can drastically change the optical transitions within the emitter by strongly modifying the vacuum fluctuations i.a. an optical cavity or a photonic crystal (PhC). Moreover by integrating QDs into different nanostructures it is also possible to increase the spontaneous emission and thus reduce the problem of high collection efficiency. Integration with nanophotonic devices also modify the spontaneous emission rate which helps minimising effects from the phonon dephasing and spectral diffusion.

In this section the theoretical description is focused on a single quantum emitter that is emitting a single photon, into an inhomogeneous photonic nanostructure. The coupling to the photonic nanostructure is described by the projected local density of states (LDOS), which quantifies the magnitude of vacuum fluctuations responsible for spontaneous emission of photons and more generally, determines the local light-matter interaction strength. LDOS is expressed as:

$$\rho(\mathbf{r}_0, \omega, \hat{\mathbf{e}}_\mathbf{d}) = \sum_\mathbf{k} \mid \hat{\mathbf{e}}_\mathbf{d} \cdot \mathbf{u}^*_\mathbf{k}(\mathbf{r}_0) \mid^2 \delta(\omega - \omega_\mathbf{k}) \tag{10}$$

where $\mathbf{r}_0$ is the position of the emitter and $\hat{\mathbf{e}}_\mathbf{d}$ is a unit vector specifying the orientation of the transition dipole moment. The mode functions $\mathbf{u}^*_\mathbf{k}$ constitute a normalized set of basis functions used to expand

the field and obey the wave equation.

The LDOS is obtained by summing over all the mode functions with eigenfrequencies ω_k that enter through a Dirac delta function $\delta(\omega - \omega_{\mathbf{k}})$ [57].

The object of interest is a solid-state QD, which in good approximation can be considered as a two-level system (TLS) which inherently emits single photons [14]. The two levels of the emitter are denoted by $|g\rangle$, ground state, and by $|e\rangle$, excited state (Fig. 6) separated by the energy $\hbar\omega_0$ and coupled to a continuum of optical modes at frequencies $\omega_{\mathbf{k}}$

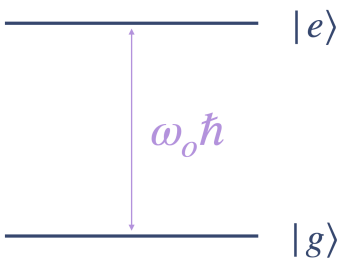

Figure 6: Energy scheme of a two-level system. Where $|g\rangle$ denotes to the ground state and $|e\rangle$ to the excited state. The energy of the transition is given by $\Delta E = \hbar\omega_0$.

The total Hamiltonian of the two level system in the rotating-wave approximation is

$$H = \hbar\omega_0\hat{\sigma}_+\hat{\sigma}_- + \hbar\sum_{\mathbf{k}}\omega_{\mathbf{k}}(\hat{a}^\dagger_{\mathbf{k}}\hat{a}_{\mathbf{k}} + \frac{1}{2}) - \hbar\sum_{\mathbf{k}}(g_{\mathbf{k}}\hat{\sigma}_+\hat{a}_{\mathbf{k}}e^{i(\omega_0-\omega_{\mathbf{k}})t} + g^*_{\mathbf{k}}\hat{\sigma}_-\hat{a}^\dagger_{\mathbf{k}}e^{-i(\omega_0-\omega_{\mathbf{k}})t}), \quad (11)$$

where the first term describes the free TLS, which has a transition energy $\hbar\omega_0$. Similarly, the second term describes the continuum reservoir of radiation modes ω_k in terms of creation and annihilation operators, $\hat{a}^+$ and $\hat{a}$. The remaining terms describe the interaction between the TLS and reservoir. Where $\hat{\sigma}_+ = |e\rangle\langle g|$ and $\hat{\sigma}_- = |g\rangle\langle e|$ are the emitter raising and lowering operators, respectively, that relate to the coherence between the states of the emitter. $g_{\mathbf{k}}(\mathbf{r}_0) = i\mathbf{d}\cdot E^*_{\mathbf{k}}(\mathbf{r}_0)/\hbar$ is the coupling rate to each optical mode, which contains the local electric field at the position of the emitter $E^*_{\mathbf{k}}(\mathbf{r}_0)$ for the mode specified by $\mathbf{k}$. There are two polarization components for each wave vector. $\mathbf{d}$ is a transition dipole moment of the emitter $\mathbf{d} = \langle g|\,\hat{\mathbf{d}}\,|e\rangle$, where $\hat{\mathbf{d}}$ is a transition dipole operator described as:

$$\hat{\mathbf{d}} = \mathbf{d}^*\hat{\sigma}_+ + \mathbf{d}\hat{\sigma}_-, \quad (12)$$

The equation of motion for the excited state of the emitter can be formulated as

$$\frac{\partial c_e}{\partial t} = -\sum_{\mathbf{k}}|g_{\mathbf{k}}(\mathbf{r}_0)|^2\int_0^t dt' c_e(t')e^{i\Delta_{\mathbf{k}}(t-t')} - i\sum_{\mathbf{k}}g^*_{\mathbf{k}}(\mathbf{r}_0)c_{g,\mathbf{k}}(0)e^{i\Delta_{\mathbf{k}}t}, \quad (13)$$

where, $\Delta_{\mathbf{k}} = \omega_0 - \omega_{\mathbf{k}}$.

This formalism is suitable for describing spontaneous emission or single-photon absorption (assuming there is a single excitation in the system). In order to derive the exact expression for a spontaneous decay rate of a single QD embedded in a inhomogeneous medium (Fig. 7) we need to describe LDOS in terms of Green function.

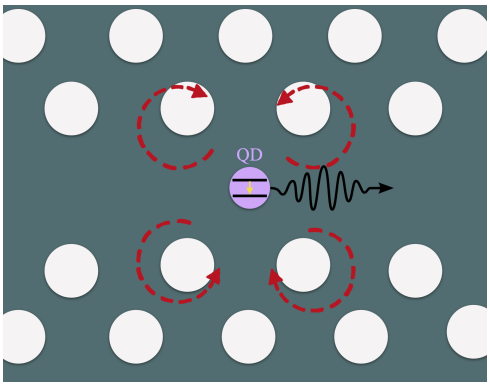

Figure 7: Scheme of spontaneous emission from a QD embedded in a photonic crystal waveguide. QD is emitting photons. The influence of the backaction of the vacuum electric field on the quantum emitter is marked with arrows.

The electric field radiated by a dipole source at $\mathbf{r}_0$ can be expressed in the Green-tensor formalism as:

$$\hat{\mathbf{E}}(\mathbf{r},\omega) = \frac{1}{\epsilon_0} \overleftrightarrow{G}(\mathbf{r},\mathbf{r}_0,\omega) \cdot \hat{\mathbf{d}}(\omega). \tag{14}$$

Based on the Eq. 14 the equation of motion (Eq. 13) can be now expressed using a Green function as:

$$\frac{\partial c_e}{\partial t} = -\frac{d^2}{2\epsilon_0 \hbar} \int_0^\infty d\omega \omega \rho(\mathbf{r}_0,\omega,\hat{\mathbf{e}}_\mathbf{d}) \int_0^t dt' c_e(t') e^{i\Delta_{textbfk}(t-t')}. \tag{15}$$

The equation above provides a complete description of spontaneous emission in any inhomogeneous photonic environment and accounts fully for the backaction of the vacuum electric field of the environment, which enters through the LDOS. LDOS is a classical quantity obtained by solving Maxwell's equations but it also determines the mode density of the vacuum electromagnetic field that is required to describe spontaneous emission.

Next we apply Markov approximation which is an assumption that the radiation reservoir is memoryless. The Markov approximation implies that $c_e(t)$ is much slower compared to the inverse bandwidth of the reservoir and allow to constitute the Wigner-Weisskopf approximation, which brings a modified equation of motion as:

$$\frac{\partial c_e}{\partial t} = -\frac{\gamma}{2} c_e(t), \tag{16}$$

where γ is the decay rate predicted by Fermi-Golden rule:

$$\gamma = \frac{\pi d_e^2 g}{\epsilon_0 \bar{h}} \omega_0 \rho(\boldsymbol{r},\omega,\hat{\boldsymbol{e}}_d). \tag{17}$$

Based on Eq. 17 decay rate is highly dependent on the LDOS, which in case of a solid state QD can be modified by embedding it to nanophotonic structures such as PhCW, which are introduced in the next chapter. To modify the spontaneous emission of a single photon emitter is crucial for engineering the light-matter interaction strength and future applications.

3

PHOTONIC NANOSTRUCTURES FOR ENHANCED SINGLE PHOTON GENERATION

So far we have introduced a properties of semiconductor QDs and their basic principles of operation. We have also mentioned that it is possible to modify the spontaneous emission of the QDs by embedding them to a inhomogeneous medium (Sec.2.6). It has been proven that embedding a single emitters into a photonic crystal waveguides (PhCW) can significantly enhance the decay rate [30] (Fig. 7). In this chapter the main characteristics of the PhCW will be presented as well as a basic description of a planar single mode waveguide.

3.1 PHOTONIC CRYSTAL WAVEGUIDE

The PhCW is realized by a two-dimensional slab photonic crystal (PhC), which is fabricated by perforating a suspended semiconductor membrane creating holes in a periodic a triangular lattice. PhCs are inhomogeneous dielectric materials where the refractive index is modulated periodically. The properties of the PhC can significantly change and control the quantum emitter embedded within. A PhC exhibit a photonic band gap which is particularly interesting for a better control of light confinement. PhC are usually used with point or linear defects to spatially confine light in the plane by photonic band gap and off-plane because of refractive index contrast [58]. Photonic band structure and therefore the bandgap frequencies depend on the size of the holes etched into the membrane, the distance between the holes, the lattice constant of the materials, the thickness of the membrane and the refractive index of the materials.
The PhCW is created by removing one row of holes from the entire photonic crystal. In the PhCW light can be confined in the plane of the membrane by the photonic crystal, and out of plane by total internal reflection on the boundary surface. By creating a line defect in the crystal, propagation of a single mode can be introduced into the photonic bandgap. The group velocity of a mode can be described by the non-linear dispersion relation:

$$v_g = \frac{d\omega(k)}{dk}, \tag{18}$$

where $\omega(k)$ is the frequency for a wave vector k. The group velocity is the speed of a wave packet of light traveling through a medium. It is significantly slower in the guided mode than it would be in vacuum. At the frequency close to the band edge the group velocity is equal to zero and therefore

the group index $n_g = \frac{1}{v_g}$ is infinity. It is not achievable in practice because of small defects such as fabrication errors or material defects which disturb the perfect periodicity of the crystal, but it can, however, exceed several hundreds. As discussed in Sec.2.6 the radiative decay rate of a QD scales with the number of modes it can emit into. When an emitter is placed inside the PhCW a change in spontaneous emission is expected due to modified LDOS. Since the density of optical states scales with the group index, an enhanced light-matter interaction is expected at the frequencies close to the photonic band edge. On the other hand, when the emitter is placed inside the photonic band gap, where no modes are allowed, the density of states drops to zero and therefore a suppressed density of states is expected, which in turn, causes an inhibited spontaneous emission. These strong LDOS modifications of the emitter embedded in a PhCW are present due to Purcell effect. The LDOS can be expressed as:

$$\rho(\mathbf{r}, \omega, \hat{\mathbf{e}}_\mathbf{d}) = \frac{n\omega^2}{3\pi^2 c^3} F_P(\mathbf{r}, \omega, \hat{\mathbf{e}}_\mathbf{d}). \tag{19}$$

where the Purcell factor F_P is defined as the ratio of the emitter decay rate at position $\mathbf{r}$ γ_{rad} to the decay rate in the homogeneous medium of refractive index n γ_{rad}^{hom} (Eq. 20) in accordance to the Purcell factor originally formulated for optical cavities [59].

$$F_P(\mathbf{r}, \omega, \hat{\mathbf{e}}_\mathbf{d}) = \frac{\gamma_{rad}(\mathbf{r}, \omega, \hat{\mathbf{e}}_\mathbf{d})}{\gamma_{rad}^{hom}(\omega)} \tag{20}$$

In PhC the Purcell factor can be either below unity (suppression of spontaneous emission) or above unity (enhancement of spontaneous) expected at the photonic band edge.

Distributed Bragg Reflector

In order to enhance and confine the emitted light from a quantum emitter a Diffracted Bragg Reflector (DBR) structure is commonly used, which is just another example of a PhCs. It is using the phenomenon of total internal reflection and is based on the interference of light reflected from successive dielectric layers.

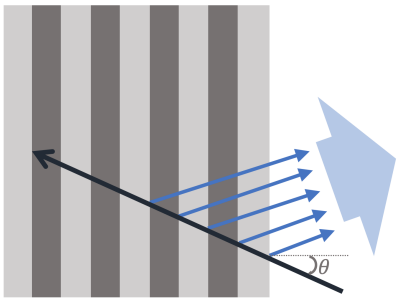

Figure 8: Interference of reflected light from multiple dielectric layers

The Bragg mirror (Fig. 8) consists of two dielectric materials with different refractive indices n_1 and n_2. The thicknesses of the layers allow the reflected waves have the same phase shift and comply with the Bragg condition for constructive interference:

$$n\lambda = 2dsin(\theta), \tag{21}$$

where n is the order of the deflection (integer), λ is the radiation wavelength, d - the distance between the planes on which the reflection takes place, and θ is the angle of incidence of the light beam on the mirror (Fig. 8).
For the chosen wavelength λ, for constructive interference to occur at the border of two materials, their thicknesses d_1, d_2 must be respectively:

$$d_1 = \frac{\lambda}{2n_1}, d_2 = \frac{\lambda}{2n_2}, \tag{22}$$

DBR is commonly used in structures with quantum devices, mainly due to the low losses of the reflected signal. Light limited by the respective DBR layers form the bottom and by the difference in refractive indices from the top is trapped in an optical cavity.

3.2 SINGLE MODE WAVEGUIDE

Single mode waveguide is one of the most popular devices building the photonic circuits. It is used to guide the light emitted from a quantum emitter embedded within. Single mode waveguide is obtained by etching a thin stripe (with a thickness in the range of a few hundred nanometers) which allows light to propagate in only one dimension, thanks to the difference in refractive indexes between the boundary surfaces (top and bottom) and between the waveguide medium and the surroundings (at the side edges of the waveguide). Optical waves propagate in the waveguide due to optical modes. Mode, in this sense, is the spatial distribution of optical energy in one (or more) dimensions that remains constant over time. Additionally, mode as an electromagnetic field must solve the Maxwell and Purcell wave equation [29]:

$$\nabla^2\mathbf{E}(\mathbf{r},t) = \frac{n^2(\mathbf{r})}{c^2}\frac{\partial^2\mathbf{E}(\mathbf{r},t)}{\partial t^2}, \tag{23}$$

where E is the electric field vector, r is the position vector, $n(\mathbf{r})$ is the refractive index, and c is the speed of light in a vacuum. For a monochromatic wave, we obtain the following solutions to Eq. 23:

$$\mathbf{E}(\mathbf{r},t) = \mathbf{E}(\mathbf{r})e^{i\omega t}, \tag{24}$$

where ω is the frequency in radians. Substituting the solution into Eq. 23 we get:

$$\nabla^2\mathbf{E}(\mathbf{r}) + k^2n2(\mathbf{r})\mathbf{E}(\mathbf{r}) = 0, \tag{25}$$

where $k = \frac{\omega}{c}$. In addition, the electric and magnetic field of the mode in the waveguide can be written by the equations:

$$E_m(r,t) = E_m(x)e^{i(\beta_m z-\omega t)} H_m(r,t) = H_m(x)e^{i(\beta_m z-\omega t)}, \tag{26}$$

where m corresponds to the mode coefficient, $E_m(r,t)$and $H_m(r,t)$ are the electric and magnetic field distributions of the mode, and β_m is the mode propagation constant. The number of modes propagating in the waveguide depends on the thickness of the waveguide and the contrast of the refractive indices.

4

EXPERIMENTAL DESIGN AND METHODS

The present chapter describes the integration of GaAs QDs into the in-plane nanophotonic structure, compatible with charge control. Moreover the technical aspects of the experiments are presented such as the experimental setup and QD excitation methods.

4.1 DROPLET QUANTUM DOTS INTEGRATED IN NANOPHOTONIC DEVICES

One of the most popular ways to fabricate QDs is using Stranski-Krastanov (SK) mode which is based on self-organization on the wetting layer. This method allows for the production of zero-dimensional structures by using the differences between the lattice constants of the substrate and the grown material (a mismatch between the crystal lattice constants should be around 15% or less [60, 61]). During the growth, the system to a certain height (critical thickness) is stressed and a continuous layer of dot material is formed with a lattice constant corresponding to the substrate material (pseudomorphic growth), and after exceeding this thickness, QDs are formed instead of a continuous layer. Since the main driving force behind the SK process is the lattice mismatch, the SK mode cannot be used to produce unstrained QDs in systems such as GaAs/AlGaAs.
Recently, advancements in the fabrication of droplet GaAs QDs allowed for a drastic reduction of the Al concentration and thus introducing a novel generation of QDs. These QDs in the bulk material are facing problems with charge noise and charge instability which lead to blinking and broad emission linewidths. Only recently the charge control of this structures has been introduced by embedding it to n-i-p diode structure [17]. The attempt allowed for significant decrease of charge noise and charge instability, making GaAs QDs blinking free. It also reduced the optical linewidths of such QDs to as narrow as the lifetime-limit.

In this section we discuss the basic characteristics of a GaAs QDs sample, a fabrication process and it's integration with into the in-plane nanophotonic structure.
All the measurements were based on semiconductor, low- strain GaAs QDs which emit light in the range of 700- 800 nm. The sample is grown on a GaAs-substrate with (001)-orientation. Below the active region, a distributed Bragg reflector is grown which reduces the scattering effects and enhances the QD collection efficiency (Fig. 9). The Bragg reflector consists of 14 pairs of $Al_{0.15}Ga_{0.85}As/AlAs$ layers. Additionally, QDs are embedded in a n-i-p diode structure where the quantum emitters are

tunnel-coupled to the n-type layer $Al_{0.15}Ga_{0.85}As$ [18]. The low concentration of Al in AlGaAs layers is crucial in order to increase the electron concentration and prevent the material to freeze out at low temperatures [62].
The QD structure has been fabricated in the Ruhr University Bochum [18].

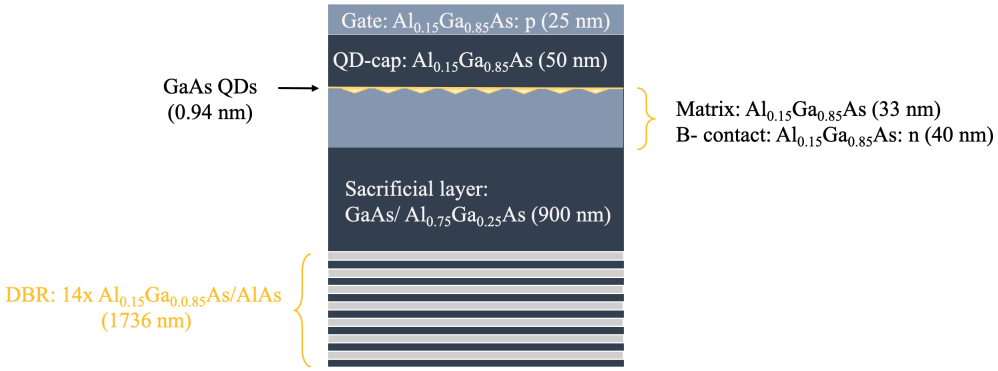

Figure 9: Design schematic of the investigated sample used during the measurements.

GaAs QDs are grown in $Al_{0.15}Ga_{0.85}As$ layer using local droplet etching (LDE). LDE is a precise and powerful technique which enables growth of GaAs QDs. In LDE, a Group III element (Al) is deposited, while the As-pressure is strongly reduced, and forms nanodroplets on the surface. With a small flux of arsenic, the droplets etch into the underlying material (AlGaAs) and form nano-holes. (Fig. 10). Etched material agglomerates around the wall surrounding the hole. Afterwards, GaAs is deposited using molecular beam epitaxy (MBE), which is well known for its high quality of the obtained structures and atomic accuracy of the thickness of the applied layers. In between the nanoholes, GaAs forms a quantum well (so-called wetting layer, in accordance with the term used in SK growth mode). The LDE method allows for high crystallinity, as well as precise control of the density, morphology, and size of QDs.

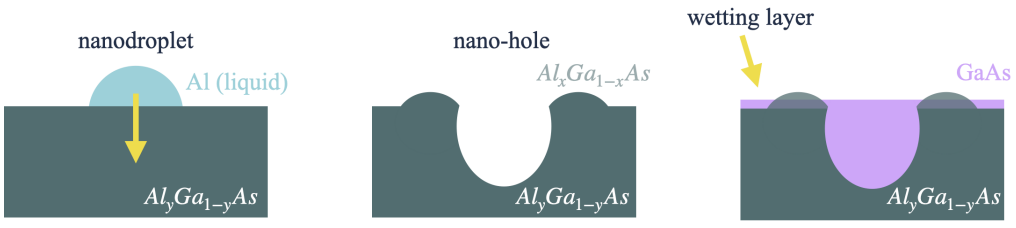

Figure 10: Scheme of QD fabrication process using LDE and hole filling.

After the growth process had been accomplished, the sample was etched in order to obtain previously designed structures using electron beam lithography (EBL).
EBL is widely used due to the high resolution- in the order of a few nanometers. It is based on scanning the surface of a sample with an electron beam, which is previously covered with a special resist. The

resist absorbs the energy carried by the electron beam, which changes the chemical properties of the material [63]. The areas scanned by the electron beam can be removed physically or chemically.
Embedding QDs into n-i-p diode and advanced fabrication technology made it possible to integrate droplet QDs into photonic nanostructures. This is the first attempt to use these structures in integrated photonic circuits compatible with electrical charge control.
Investigated QDs were embedded in photonic devices consisting of shallow etched grating (SEG) couplers, waveguides and photonic crystal waveguides (PhCW) designed for adequate spectral range. The QDs are located at the central layer of the membrane, and coupled to the waveguide along the x axis (Fig. 11). The waveguides are fabricated along one of the crystallographic axes defined during the growth, such that the dipole orientations are aligned with either x or y direction. The light going into or out of the waveguide is coupled using SEG couplers terminating the waveguide in each end. A 2D slab photonic crystal is used, which is fabricated by perforating a suspended semiconductor membrane creating holes in a periodic a triangular lattice. The waveguide is created by removing one row of holes from the entire photonic crystal, as sketched in Fig. 11.

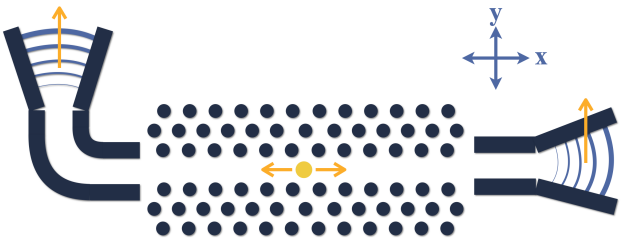

Figure 11: Sketch of a device used during the measurements. A photonic crystal waveguide, which collects the emitted photons from the QD, and guides the photons to the shallow etched grating out couplers.

To investigate the integration of GaAs QDs and to characterize the photonic nanostructures the fabricated sample contained of a nanobeam waveguides and PhCWs. All the devices were optimized for QD emission at 785 nm.
Nanobeam waveguide is a device embedded between two SEGs couplers (Fig. 12a). On the sample nanobeam waveguides differed in the width of the waveguide (280, 290, 300, 310, 320 nm). The another photonic device used the measurements- PhCW is a devices which guide the light within the photonic crystal (Fig. 12b). The fabricated PhCW devices differed from each other in the radius of the holes in photonic crystal r (32, 33, 32, 31, 30, 29 and 28 nm) as well as the lattice constant a (203, 204, 206, 208, 210 nm).
In order to ensure that all quantum devices with different parameters could be measured, each device on the sample was repeated several times. This guarantees the success of the measurement in the event of a breakage of the waveguide or SEG.
The transmission of a nanobeam waveguide and a PhCW was determined. The average transmission of a nanobeam waveguide $< \theta_{NB}(\lambda) >$ (Fig. 13a) was measured for four different devices with the same width of the waveguide of 300 nm.
The standard deviation was estimated as: $d\theta_{NB}(\lambda) = \sqrt{\frac{sum_i(\theta_{NB,i} - <\theta_{NB}>)^2}{N-1}}$, where N is the number

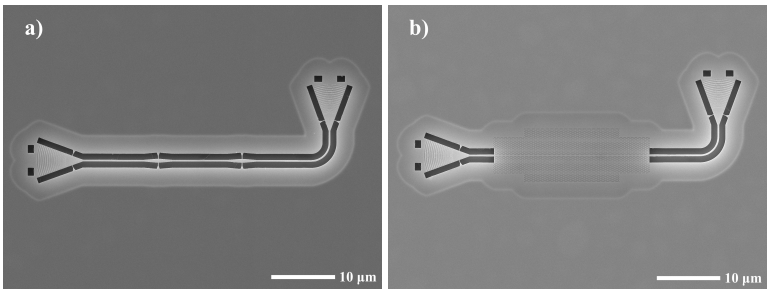

Figure 12: Scanning electron microscope (SEM) images of a) nanobeam waveguide and b) PhCW.

of measured devices.

The average transmission of a nanobeam waveguide revealed that the transmission window for this device is between 750- 810 nm, with the maximum transmission at around 780 nm.

Analogously, a transmission of a PhCW with a lattice constant 205 nm and the radius of hole equal to 46 nm was measured. The obtained transmission spectra of a PhCW was divided by the average nanobeam waveguide transmission in order to inspect the influence of the photonic crystal on the transmission (Fig. 13b). The width of the transmission window for PhCW is in the similar range with a characteristic cutting edge value at around 814.8 nm and maximum transmission around 810 nm. The cutting edge value corresponds to the wavelength at which the Purcell factor has the highest value and therefore an enhanced spontaneous emission rate of a QD at this wavelength is expected. The cutting edge depends on the properties of the PhCW (a lattice constant and a size of holes).

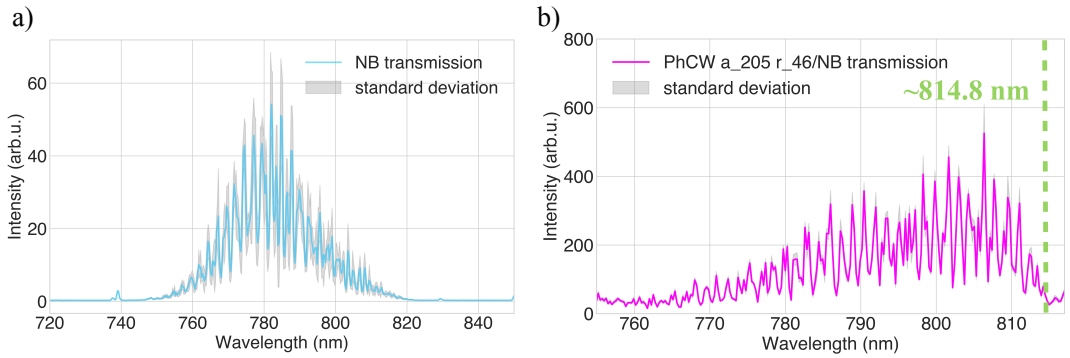

Figure 13: A transmission of photonic devices a) the average transmission of a nanobeam waveguide device b) the transmission of a photonic crystal waveguide with a lattice constant of 205 nm and radius of a hole equal to 46 nm divided be the average transmission of a nanobeam waveguide.

The nanobeam waveguide and the PhCW were measured on different sample with the same QDs structures, however a lattice constant and a hole size of a PhCW were different.

4.2 QUANTUM DOT EXCITATION IN PHOTONIC DEVICES

Different excitation methods can give a deep insight into the electronic structure and optical properties of quantum emitter. Some of the most popular excitation methods which were also used during the measurements for the thesis are described below.

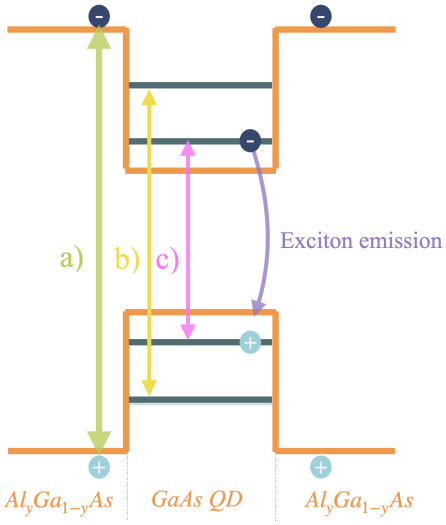

Figure 14: Three main excitation schemes (a) aboveband, (b) quasi-resonant, and (c) resonant optical excitation scheme.

On Fig. 14 some of the basic excitation methods of a QD are presented. Depending on the energy of the excitation laser we can excite a QD using aboveband excitation (the energy of the excitation laser is much higher than the energy of the substrate) (Fig. 14a), quasi- resonant excitation (through higher energy states) (Fig. 14b) or resonant excitation (energy of the excitation laser is in resonance with the band gap energy of a QD) (Fig. 14c).
For investigated structures the typical aboveband excitation energy should be between the band gap of $Al_{0.15}Ga_{0.85}As$ (770 nm) and AlAs (574 nm) [64] or lower. Droplet GaAs QDs have been widely studied using 520 nm aboveband excitation [65].
The excitation through the higher order QD electron configuration (p-shell, d-shell etc.) will lead to emission through the s-shell via fast phonon relaxation (as shown on figure 14b). Previously the GaAs QD emission was characterized at the room temperature 250K, where the s-shell resonance at 1.479 eV (838.3 nm) was measured, while the p-shell resonance is shifted by 52 meV ([66].

The mode of the waveguide can also be used to excite the QD embedded into it. For this the SEG coupler can be used to couple the excitation light into it and collect the QD emission after. The experimental setup has been modified such that it is possible to excite a QD embedded in the PhCW either out-of-plane (perpendicular to the waveguide plane) or through the SEG in transmission (Fig. 15).
QD excited from the top can emit light in both directions of the waveguide. The light therefore propagates to the both ends to SEGs. The transmitted light is reflected on the trenches and thus only light with vertical (or horizontal with respect to the waveguide) polarization will be reflected out-of-plane.

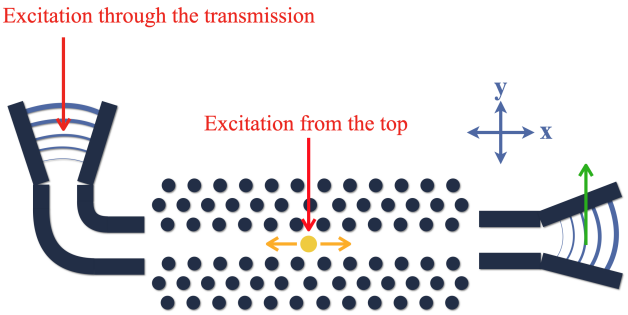

Figure 15: A QD excited with laser from the top or through the transmission (red). QD can emit light in both directions in the waveguide (orange). Emission can be collected from SEGs (green).

Excitation Methods

4.2.1 *Aboveband excitation*

The aboveband laser (ABB) excites a QD non-resonantly with energy higher than the band gap of the substrate material. In the case of an electron in a semiconductor material, under the influence of the photon absorption, it is excited from the valence band to the conduction band, thus creating an empty space left by the electron, the so-called a hole, positively charged quasiparticle, in the valence band. The electron and a hole are attracted to each other by the electrostatic Coulomb force, creating an exciton (Sec.2.2). The excited carriers relax to the lowest energy levels (or defect states) through interaction with phonons, and recombine emitting a photon of a specific wavelength or non-radiatively, e.g. through the Auger process (excess energy is transferred to an adjacent carrier) or interaction with phonons (energy is released as heat). The relaxation of carriers to the lowest energy levels makes it difficult to observe emissions from higher energy states.

In order to minimize the influence of interaction with phonons, the investigated structure can be placed in a cryostat and its temperature is lowered to the cryogenic temperature (most often liquid helium temperature 4.2 K) [67]. This is especially important when we want to study individual nanostructures such as a QD.

ABB due to its high power and wide range allows to excite a multiple QDs which can be visible in the same spectrum. It can also excite a multiple states in a single QD which makes possible to investigate the electronic structure of the quantum emitter. However, if only analysis of a single QD is required, the ABB can be not sufficient since the carriers will diffuse to neighboring QDs and pollute the spectra. In this case the single photon indistinguishability is lost due to dephasing, which comes from the fluctuations of the electrostatic environment around the QD. This can be neutralized by turning down the laser power significantly or using a different excitation method [68].

By increasing the temperature during measurements, it is also possible to look into the influence of interaction with phonons on the emission spectrum, determine the activation energy of carriers or determine the value of the band gap of the investigated material at a given temperature (for a bulk

material).
Since the QDs can also be embedded in the diode it enables to perform the measurements as the function of applied external electric field to the structure. Due to Stark shift the electronic structure modifies which shift and split the spectral lines of the QD.

4.2.2 *P- shell/ quasi-resonant excitation*

A quasi-resonant excitation helps to improve a QD single photon indistinguishability, as the carrier capture process is eliminated and phonon assisted carrier relaxation is minimized. A quasi-resonant exciton is using a laser source which wavelength is resonant to one of the high energy state of the QD. One of the most efficient ways to excite a QD is when the laser has the same energy as p-shell state (52 meV with respect to the s- shell [66]). The p-shell excitation enables controlled occupation of one electron–hole pair in the p-shell. After relaxation into the s-shell, each generated electron–hole pair emit a single photon. Therefore high quantum efficiency can be possible [69].

4.2.3 *Phonon assisted excitation*

One of the popular ways to efficiently excite single QD is to use the neighboring phonon states. Usually the interaction of QD and phonons has negative impact as it causes broadening of the emission line. On the other hand phonons can also interact with QDs, through inelastic scattering with the bulk phonons of the material. Therefore the QD can be excited to the s-shell via excitation accompanied by the phonon emission which leads to a rapid photon emission. The fast decay time leads to a broad emission spectrum around the exciton transition. From the photon emission accompanied with a phonon emission a phonon sideband appears. This excitation method of a single QD can significantly reduce noise from neighboring QDs. An example spectra of a phonon assisted excitation is shown on the Fig. 16.
Using phonon assisted excitation only a single emission line from a QD is visible. The laser was filtered using a polarization optics on both excitation and collection path (Fig. 18).

4.2.4 *Resonance Fluorescence (resonant excitation)*

In order to perform resonance fluorescence the laser frequency must be selected with extremely high accuracy which corresponds to s-shell state (784.91 nm at 18K). Even the smallest fluctuations in the laser frequency (in the range of a few GHz) and polarization can significantly affect the effectiveness of a QD excitation. Since the excitation and an emission are at the same frequency, it makes it very difficult to distinguish the signal on the spectrum. Many techniques has been introduced in order to filter the laser signal from the spectrum [70, 71]. One of the most popular techniques is to use the cross polarization configuration where the laser with a given polarization is filtered using polarization optics which transmit only the light that is perpendicular to the laser [72].

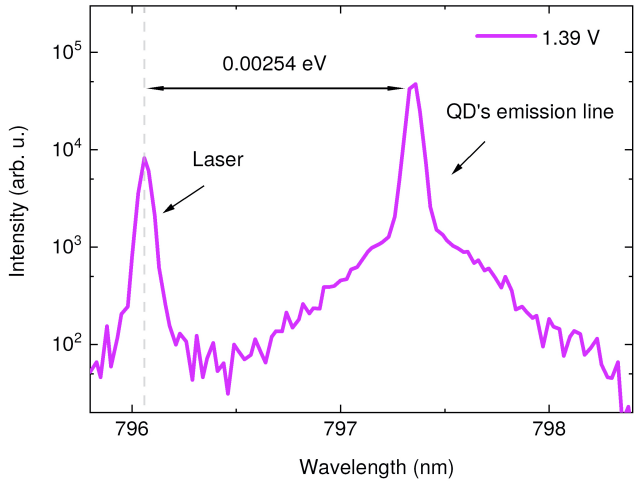

Figure 16: A phonon assisted excitation of a QD. The distance between the laser and a QD's emission line at around 2.54 meV.

Exciting a QD embedded in PhCW might be more challenging due to Purcell enhancement which increases optical density of states which it can emit into. Due to Fermi's golden rule for spontaneous emission, the oscillator strength to other modes is decreased, so exciting a QD in PhCW requires more power, comparing to a QD in the bulk material.

A typical spectra for RF is shown on Fig. 17. The laser frequency is set at the resonance with QD emission. The QD emission is visible when the voltage is turned on at 1.4V. When the voltage is set to 1V (referred as „Background" on Fig. 17) the QD is not excited. The spectrum of the QD was filtered using filter grating and detected on APD detector (see Sec.4.3).

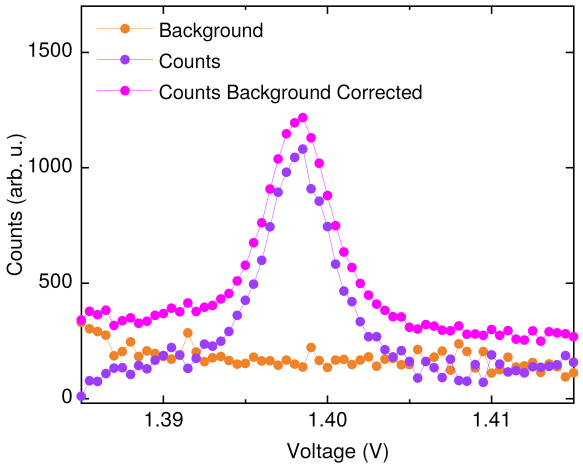

Figure 17: A typical RF spectra measured on APD detector. The background (orange) is measured for reference 1V when QD is not excited. After turning on the voltage at around 1.4V the counts (purple) are detected on the APD detector.

Despite the difficulties in using RF, mainly due to laser light leakage [73] low $g^{(2)}(0)$ were achieved via in-plane photon crystal waveguide platform [24].

4.2.5 *Resonance Transmission*

Resonance transmission (RT) in comparison to the other excitation techniques described above, excite the QD through the transmission along the waveguide. The laser frequency, in analogy to the resonance fluorescence, must be in the same frequency as the QD emission in order to perform a measurement. Coherent interaction between the electric field of the laser and QD reflects light which is in resonant with the QD. Since the light in resonance with QD is reflected instead of peaks in the spectrum, we can observe a dips. By tuning the laser across the QD resonance and recording the transmitted signal, we can identify the spectral location of all QDs coupled to the waveguide.
During the project a transmission resonance measurements were preformed, however an emission from QDs was not observed.

4.3 HIGH-RESOLUTION AND TIME-RESOLVED OPTICAL SPECTROSCOPY

In order to investigate and characterize the structure a high resolution optical setup with two excitation ports (excitation from the top and through the waveguide) was utilized (Fig. 18). The sample was mounted in the closed- cycle cryostat and cooled down to cryogenic temperatures (around 7K) in order to reduce the inelastic interaction with the phonon bath in the QD coupled to photonic crystal waveguide. The cryostat was additionally mounted on piezo stages which enabled scanning the sample at different areas. When measuring single QDs in a photonic devices, an elements used to preview the sample surface also play an important role. It allows to find the desired structure or a system. The part of the setup used to view the sample surface consists of a white light source, a CCD (charge-coupled device) camera and a focusing lenses. Before a CCD camera a long pass 800 nm filter was used in order to filter the laser beam from the image in case of aboveband or quasi resonant excitation. Along the excitation path, light passes through an objective with a magnification of x100 and a numerical aperture of 0.85. The emitted light goes back through the same objective and is collected through the fiber and detected using an APD detector or through the spectrometer on the CCD camera. Before the detection of the signal the spectral filtering was applied when necessary $(Fig.18)$. On both excitation and collection paths a polarization optics (half wave plate (HWP), quarter wave plate (QWP) and linear polarizer) was used.
Additionally, the transmission of the setup after each element was measured using the laser beam at 795 nm (average QD emission wavelength) and the results are shown in Table 1.
From the measured laser power transmission, the transmission of the objective of 68 % was estimated. From the power transmitted through the system it was also possible to determine the transmission efficiency of the SEG (the fraction of light diffracted by the SEG outcoupler) which for the investigated device is around 60%. It result in around 25% collection efficiency from the PhCW into the fiber.
In order to resolve the QD spectrum from the excitation laser a grating filter setup was utilized. It is built in 4f configuration consisting of two negative and two positive lenses with focal lengths of -50 mm and 200 mm respectively (Fig. 19). The beam after the first pair of lenses is expanded which

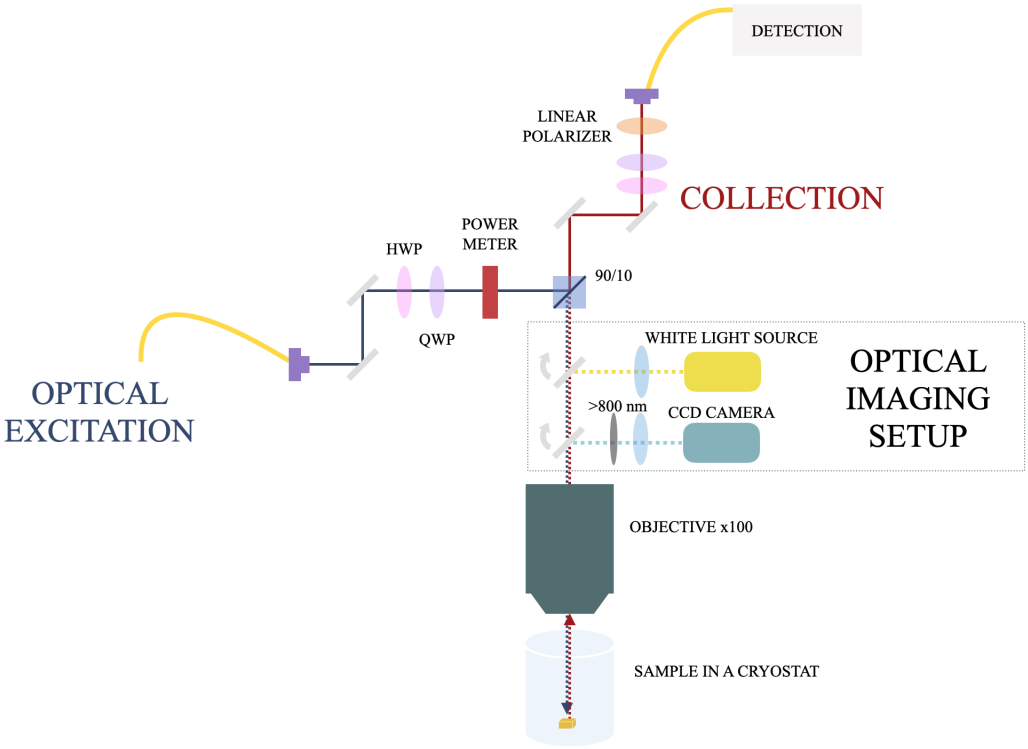

Figure 18: A schematic of an optical setup used during the measurement.

ensures higher spatial resolution between different frequency components in the Fourier plane when imaging the reflected beam. The beam is transmitted towards the grating. Diffracted light is next directed on the lenses which focus the light and to the fiber coupler. Only a certain wavelength range is collected. The measured FWHM of the setup is 21.64 ± 0.13 GHz.

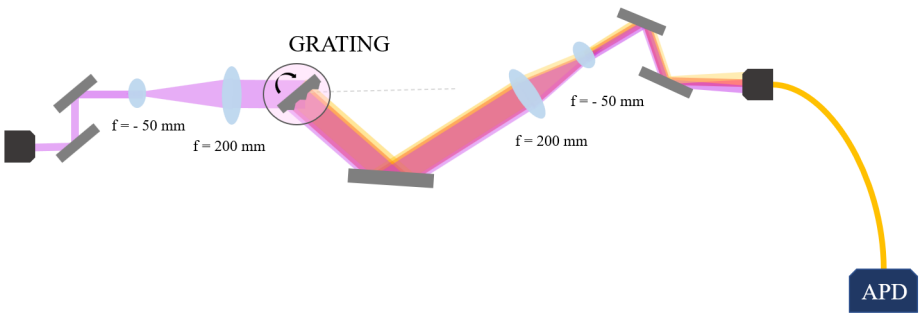

Figure 19: Scheme of a grating filter setup.

The transmission of the grating filter setup is $72\% \pm 3\%$ and the fiber coupling is in the range of $50\% \pm 4\%$.

Part of the optical set up	Laser power (mW)	Transsmited light
laser input	3.3	100%
after fiber coupler	2.1	63.64%
before polarization optics	1.2	36.36%
after polarization optics	0.55	16.67%
before objective	0.067	2.03%
after objective (collection)	0.021	0.64%
before fiber coupler (collection	0.013	0.39%
after fiber coupler (collection)	0.0026	0.08%

Table 1: The transmission of the optical setup. A power of 795 nm laser was measured after each element of the optical setup.

4.4 EXCITATION AND COLLECTION EQUIPMENT

In this section the hardware used for excitation and collection are described. Firstly, the excitation lasers used during the measurements are introduced and next, detectors used for the QD emission collection are briefly described.

a) DLPro

In order to perform a measurements on GaAs droplet QDs a set of adjustments in the set-up had to be performed. The main step was to implement a new, tunable in the range of 765- 805 nm, continuous wave, narrow line-width diode laser- DLPro. The laser frequency is motor operated and additionally, the laser diode is mounted on a piezo element which allows extremely fine tuning of the laser frequency.
The tuning range enables to perform measurements using quasi- resonant (p-shell) and resonant excitation. Most of the measurements in the thesis were carried out using DLPro laser.

b) Tsunami

Ultrafast Ti:Sapphire Oscillators- Tsunami laser, was used for the pulsed excitation. It is tunable in the range of 700- 1080 nm. It is a high power laser with regenerative mode-locking mechanism which provides a long-term stability. The tuning range of the laser, in accordance with DLPro, enable for quasi-resonant and resonant excitation. The pulsed laser was especially important when performing life-time and second order correlation function $g^{(2)}(\tau)$ measurements.

c) HeNe laser

A helium–neon (HeNe) laser was used during the measurements for ABB excitation. It's a sim-

ple gas laser which high energetic medium gain medium consists of a mixture of helium and neon gases. It emits light at around 635 nm. Since the wavelength of the laser was not very efficient in excitation of GaAs QDs, it did however enable to create a „QD map" on our sample. The high power was exciting neighboring QDs which was visible on the camera in the setup. See more in Chapter 6.

d) Collection: Spectrometer and photodetectors

All the spectrum measured on the spectrometer were using high resolution 1200g/mm grating. Spectrometer which is using CCD enable to record the full spectrum which for the grating given above is in the range of around 40 nm. It helps to distinguish and identify a single QD lines as well as align the QD emission with the excitation and collection ports for high collection efficiency.
In comparison to spectrometer, the Avalanche Photo Diode (APD) cannot see the full spectrum, it simply detects and counts photons using photoelectric effect. The efficiency of APDs at 800 nm is around 60%.

5

CHARACTERIZATION OF NANOPHOTONIC PLATFORM FOR DROPLET QUANTUM DOTS

In the previous chapter we have focused on the technical aspects of the setup as well as design of the investigated sample. In this chapter the experimental characterization of the sample is presented.
In the first steps the basic characterization of the nanophotonic platform is made. The I-V curve of the diode is measured to reveal the gate turn on voltage. Next the propagation losses in a nanobeam waveguide are estimated.
As mentioned in Sec.4.1 the investigated GaAs QDs were embedded in a quantum devices based on a nanobeam waveguides and a photonic crystal waveguides. The general sample and setup characterization is followed by the investigation of a single QDs.

5.1 ELECTRICAL CHARACTERIZATION

In this section we show the measured impedance of the n-i-p diode in which investigated droplet GaAs QDs were embedded.

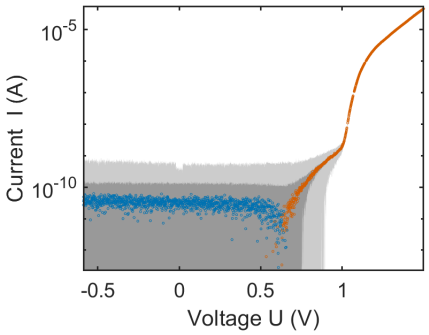

Figure 20: Current-voltage (I- V) characterization of the p-i-n diode measured at cryogenic temperature 6K. Absolute current with sign in color of data points- positive voltages (orange) and negative voltages (blue). Dark gray: Systematic error of Keithley 2450. Light gray: standard deviation of single measurement. 100 Samples taken per point.

A n-i-p diode structure enabled a constant electric field across the active layer between n (negative) and p (positive) layers. The diode was made directly during the GaAs growth and additional AlGaAs barrier was added in the intrinsic i region to prevent current flow in the membrane. The strength of the field determines the steepness of the slope of the conduction and valence bands and can be changed

by applying an external field. The external voltage was carefully controlled using a Keithley 2450 Source-meter in 4-wire configuration with a Ultra Low Noise low pass filter (10Hz Cut-Off) were used to control the voltage across the diode. In order to connect the sample with the control device a wire bonding on the metal contacts was performed.
The impedance of the diode was measured which revealed that design turn on at the gate voltage is around 0.9V at 6K (Fig. 20).
Most of the measurements were performed at around 1.4V where the diode current density is much higher than at the gate turn on voltage at 0.9V. This might cause an unstable charge environment and therefore a spectral broadening. Ideally, the measurements should be performed with the bias voltage as close to gate turn on as possible, however it was very difficult to measure QDs at this voltage since the emission intensity of the emitters was extremely low.

5.2 PROPAGATION LOSSES IN THE WAVEGUIDE

The transmission of the nanobeam waveguides is limited by the propagation loss [74]. To fully characterize the emission from the QD and verify the functionality of the system, it is important to determine experimentally the intrinsic propagation loss.
Signal losses can be attributed to three different mechanisms: scattering, absorption, and radiation. In general, the waveguide attenuation T in decibels (dB) is expressed as the ratio of the power P as a function of the distance traveled by the signal in the propagation direction (z) to the power received at the output of the waveguide P_0:

$$T(dB/mm) = \frac{10log_{10}(\frac{P}{P_0})}{z}. \tag{27}$$

Scattering losses
In an optical waveguide two different types of scattering might occur. The first is related to light scattering on imperfections in the waveguide volume, i.e. crystal defects, interatomic spaces or impurities. This type of scattering depends on the relative size of the imperfection compared to the wavelength propagating in the waveguide, but usually the losses are so small that they can be neglected. The scattering on the waveguide surface is much more important. The scattering occurs mainly due to the roughness of the waveguide surface, which is caused by the difficulty of fabricating small objects with high resolution.

Absorption losses
Absorption losses are the main problem in waveguides made of semiconductor materials due to interband absorption and inband absorption. In order to avoid absorption between bands and limit losses in the waveguide, the material of the waveguide must be selected adequately for the energy of propagating wavelength. Free carrier absorption losses mainly occur when the waveguide limiting substrate or layers are heavily doped.

Radiation losses

A portion of the light propagating in the waveguide may be radiated beyond the medium area of the waveguide and will no longer be transmitted. These types of losses can be neglected in the case of straight waveguides when the signal is transmitted parallel to the axis of the waveguide, but play a large role when the waveguide is bent. Due to the distortion of the optical field during the transmission of light through the bent waveguide, the losses significantly reduce the power of the transmitted light.

The transmission of the nanobeam waveguides of different lengths, which are fabricated on the same sample as a PhCW, was measured (Fig. 21). The transmission of 11 devices was measured for a constant power of the laser with the QDs switched off (the column is not connected to a voltage source). In order to measure the transmission of a nanobeam waveguide a SuperK laser was used. The NKT Photonics Supercontinuum ”SuperK” laser, produces a spectrum from 410-2400 nm, which enables to receive a complete transmission spectrum of a photonic structure (limited by the resolution of the spectrometer). Fig. 21 shows an integrated and renormalized transmission.

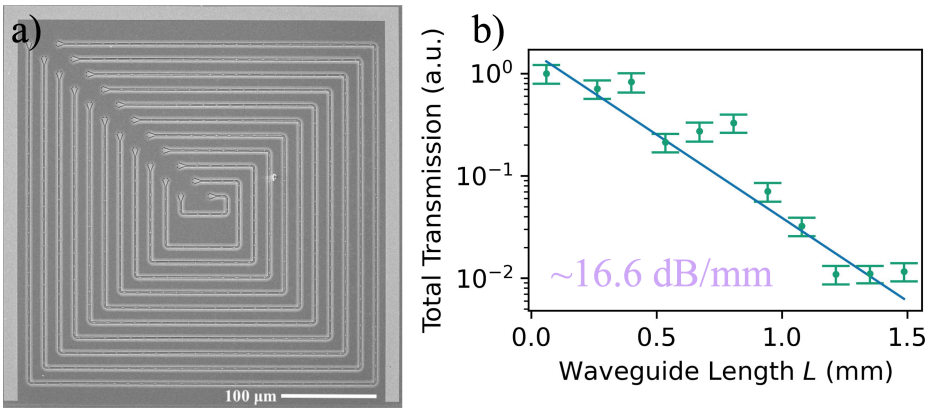

Figure 21: Propagation loss of a nanobeam waveguide a) SEM image of nanobeam waveguides of different lengths, b) dependence of the transmission on different nanobeam waveguide length. Data points fitted with linear regression.

The obtained dependence of transmission on the waveguide length was fitted with a simple linear regression and it was possible to determine that for a nanobeam waveguide the losses are around 16.6 dB/mm. The attenuation of the nanobeam waveguide in the tested structure, optimized for the highest transmission of GaAs QDs at 790 nm, is much higher compared to the typical GaAs samples where the propagation loss are around 10 dB/mm [75].

One of the reasons for such high attenuation of tested structures is the scattering of light on rough surface of its side walls due to the imperfections of the technique used to etch devices in the semiconductor structure and the non-optimal selection of parameters during etching. With such a small waveguide size (the width of the waveguide is around 300 nm), the surface to volume ratio is high, making surface irregularities play an increasingly important role and optimizing the etching process is even more important [76, 77].

The absorption of light by the GaAs substrate also contributes significantly to the attenuation of the waveguide. As described in Sec.3.2, this type of waveguide loss occurs very often in semiconductor materials and also affects the waveguide attenuation. Additionally the propagation losses are also caused by the Franz-Keldysh electroabsorption in n-i-p junctions. When applying an electric field through the semiconductor junction, the wave functions of electrons and holes are deformed and can overlap with the band gap. Therefore an absorption of a photons with energy lower than the band gap is possible, which can affect significantly the propagation losses of a waveguide [74].

6

OPTICAL CHARACTERIZATION OF DROPLET GAAS QUATUM DOTS

In this chapter we investigate an optical properties of a single GaAs QD.
Firstly, in Sec.6.1 the basic optical properties of a QD in a bulk material were measured using aboveband excitation. This results are followed by the characterization of a selected single QD in a photonic crystal waveguide in Sec.6.2 (the dependence of the emission on the applied bias voltage which enables to determine Stark shift and dependence of the emission on the excitation power to identify the exciton state) using different excitation methods. These measurements are followed by more advanced experiments such as resonant fluorescence and autocorrelation $g^{(2)}(\tau)$ measurement. The time resolved spectroscopy is also performed in order to determine the lifetime of an exciton within a QD.
Measurements are performed in two different temperatures. At first, the measurements are performed with a sufficient thermal anchoring to an unknown sample temperature marked as XK (temperature estimated between 15- 20K). A higher temperature may be caused by limited thermal connection of the sample with the cold finger in the cryostat due to poor thermal contact. To estimate the temperature dependence of the resonance frequency a linewidth of the QD is measured and compared to the values found in a literature. After fixing the issue, the rest of the measurements are performed in 7K. A difference in spectrum for these two temperatures are shown on the example of a QD embedded in a photonic crystal waveguide. For most measurements the DLPro laser was used which enabled a quasi resonant as well as a phonon-assisted and a resonant excitation. As a pulsed excitation source a tunable Tsunami laser and the Mira laser are used. All measurements are performed by exciting a QD from the top (out-of-plane) and detecting the collection through the SEG out coupler.

6.1 QUANTUM DOT IN BULK MATERIAL

In this section the characterization of a single QD in bulk material is presented. It is difficult to measure QDs in bulk material since the emission is not guided into any mode and can be easily scattered and lost. The characterization of QDs in bulk material can however show a typical behaviour of the investigated QDs, such as a turn on voltage and emission spectral range.
The first approach to characterize QDs was based on above-band excitation using a HeNe laser emitting at 632nm. For a very high excitation power it was possible to observe that all neighboring QDs are „turning on” in the high bias voltage regime at around 1.4V and appear on the camera

image of the sample surface (Fig. 23). The setup for camera image of the sample surface is directly connected to the main setup. It is based on a white light source and a CCD camera, in front of which there are focusing lenses. In front of the camera an additional short pass 800 nm filter was used which filtered the laser beam light on the image (Fig. 18). This feature enabled to create a „QD map" where it is easy to identify a single QDs.

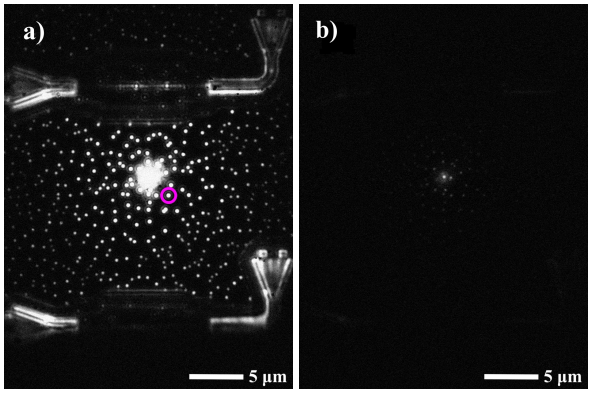

Figure 22: Camera image of a sample surface a) for applied voltage 1.4V. A pink circle marked as a selected QD position in a bulk material. b) for applied voltage 0V.

As shown in Fig. 23 after turning on the voltage to 1.4V the emission of the individual QDs is visible on the camera image. Due to a long pass 800 nm filter the laser beam is significantly reduced and is not saturating the image. In the Fig. 23a it is visible that the QD density is close to the estimated QD density on the wafer- $2\mu m^{-2}$. Bright QDs are visible not only in bulk material, but we can also identify QDs in a nanophotonic devices. On Fig. 23a QDs coupled to a photonic crystal waveguide are visible. The bright spot in the middle is the excitation laser beam focused on the sample surface. For a selected QD an applied bias voltage dependence on emission spectrum was performed (Fig. 24). The measurement was conducted using a HeNe laser at 250 μW (power measured before 90/10 BS as shown on Fig. 18).

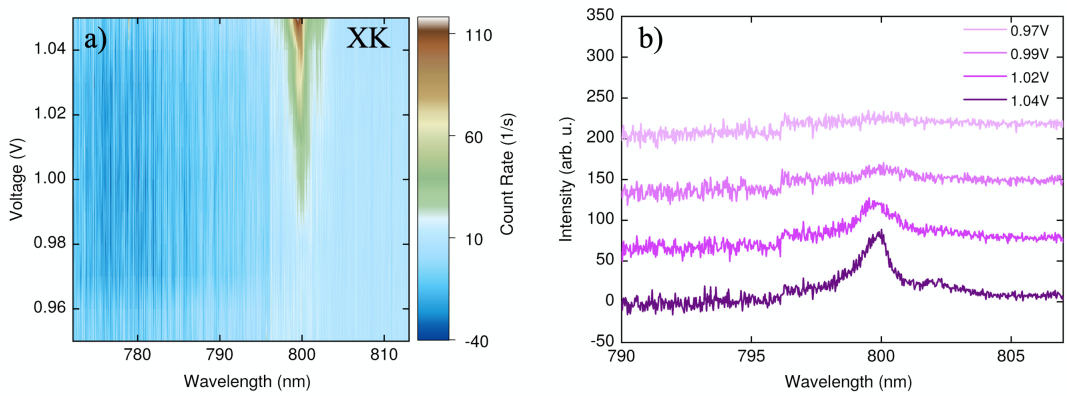

Figure 23: The spectrum of a selected QD in a bulk material as the function of applied voltage a) a spectrum map of a QD emission b) a QD spectra for selected voltages. The measurement performed using an aboveband excitation with 250 μW measured on the power meter (Fig. 18) at XK.

What is worth noticing is the fact that QD's emission is still visible below 1V. From Fig. 21 the estimated turn on gate voltage is around 0.9V. The closer we can get to this value the less charge noise (which for semiconductor structures mainly origins from occupation fluctuations of the available states and leads to fluctuations in the local electric field [78]) is expected on the spectrum.
The measurement was performed at XK and the emission line appeared at around 799 nm. The QD in a bulk material was excited from the top and its emission was collected from the same spot. The spectral broadening and a low intensity of QDs in bulk material made it impossible to continue with further characterization. For this reason in the next chapter we proceed with characterization of QDs coupled to nanophotonic structures.

6.2 QUANTUM DOT INTEGRATED IN A PHOTONIC CRYSTAL WAVEGUIDE

A single-photon source has a strict requirements of high efficiency (brightness) and high single- photon emission rate in order to perform in quantum based technologies such as quantum communication or quantum computation.
In this chapter a selected single GaAs QD (QD1) embedded in PhCW (Fig. 24) is introduced and characterized as a potential single photon source. The selected QD1 was coupled to a device with a lattice constant of 206 nm and with a radius of the photonic crystal holes equal to 36 nm (Sec. 4.1.). QD1 was characterized in two different temperatures. First, the measurements were performed at a higher temperature XK Sec. 6.2.2 (estimated between 15- 20K) and later at a cryogenic temperature of 7K Sec. 6.3. The obtained results from measurements performed at both temperatures are analyzed and compared.

Quantum dot at XK

Due to poor thermal connection the first measurements were performed in higher temperature marked as XK (estimated between 15- 20K).
A brigth QD1 was selected due to its high intensity and relatively narrow linewidth comparing to other QDs embedded in PhCWs.

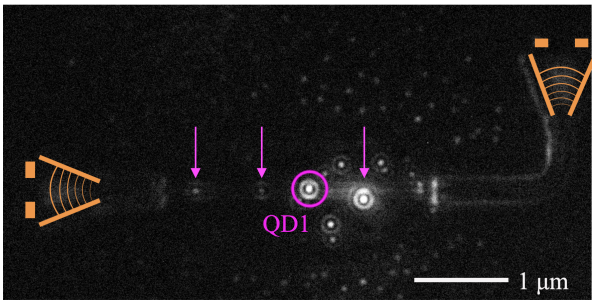

Figure 24: Selected QD1 marked with a pink circle coupled to the PhCW device. The neighboring QDs marked with an arrows. With orange lines the SEG couplers are marked.

On Fig. 24 the spatial position of a QD1 is marked as well as the position of neighboring QDs in the same device. The emission from the quantum emitter is coupled to the photonic crystal waveguide and is collected from the SEG outcoupler.

Firstly, the QD1 was characterized by the dependence of the emission spectrum on the applied voltage. It was measured using quasi-resonant excitation at 784.91nm. The signal was detected using the CCD camera of the spectrometer. It revealed the spectral tuning of the QD and how bright is the QD depending on the applied voltage as well as various charge states of the QD (Fig. 25a). Both the excitation path (the position and the wavelength at 784.91 nm of the excitation laser) and the collection optics were optimized for the highest collection efficiency of the QD1 at 1.4V (emission line wavelength at 799.1 nm).

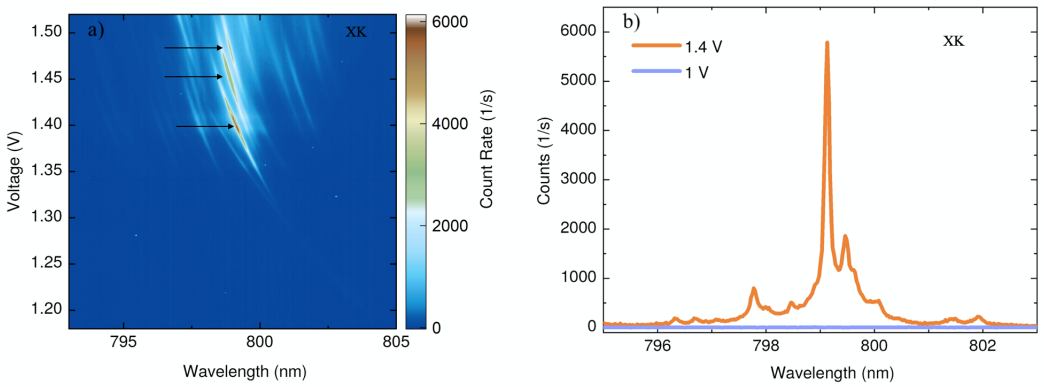

Figure 25: QDs in PhCW excited quasi resonantly with 784.91 nm and 100 μW power . Measurement performed at temperature XK. a) Emission spectras measured at different applied voltages. Emission from a QD1 marked using black arrows. b)The spectrum of the QD1 in the W1 with applied voltage of 1.4V and 1V.

The measurement performed for 784.91 nm excitation wavelength revealed the maximum counts at 1.4V in the range of 6000 counts/s. The two other marked lines which have a maximum at a higher energies probably corresponds to the other excitonic charge states of the same QD1. Once one of the lines with a higher energy starts to drop- minimize the counts, the another line is increasing in counts. Similar behavior of droplet QDs has been recorded in [17], where positive trion, the neutral exciton, and the negative trion were identified in the photoluminescence of a QD as a function of the gate voltage.

Additionally, on the spectrum map a neighboring QDs are visible. the tuning slope of these dots is different and their intensity is not as bright as selected QD1. This is due to fixed laser excitation point adjusted for the position of QD1. These QDs coupled to PhCW are also visible on the „QD map" on Fig. 24. For each of the lines marked with black arrows (Fig. 25a) satellite lines are observed with lower and/or higher energy. These lines presumably are the result of tunneling transport of charges through the diode. Further investigation would be needed to confirm the physical mechanisms of their generation.

The charge noise is usually visible in a high voltage regime where the Coulomb interaction of many-particle states including electrons and holes in the individual QDs, as well as the interaction between

neighboring QDs and the charges from the layers below is enhanced [79].
On Fig. 25b a spectrum of the QD1 is shown when the applied bias voltage is equal to 1.4V and 1V. On the QD1 spectrum a narrow emission line is visible for an applied bias voltage of 1.4V. The broadening of the spectrum can be caused by the phonon interaction due to high temperature and by overlapping the spectrum with neighboring QDs. The small lines on the left side of the main peak probably origin from a different charge states.
Investigated QDs are highly sensitive for a Stark Shift tuning. Since the emission wavelength is moving towards higher energies along with applied voltage it is also more difficult to distinguish the emission line for lower voltages (below the voltage that QD was aligned for). The optics used in the setup would also need to be aligned for different emission wavelength. Moreover, the Stark Shift also changes the p-shell energy (and other energy states) therefore the excitation wavelength in this case should analogously be tuned towards the higher energies with the applied voltage. The QD1 was aligned for 1.4V since the emission at that voltage was the highest.

In order to estimate the Stark Shift, for each applied voltage the adequate emission spectrum (from Fig. 25a) was fitted. Since in each spectrum a multiple lines are visible a multiple Voigt function was used for fitting the emission lines. Obtained peak intensities from the fit were next plotted as a function of bias voltage tuning (Fig. 26). The obtained dependence was fitted using simple linear function for low voltage tuning when we omit the polarizability. The slope of linear regression is the sought Stark Shift of 6.200 ± 0.045 (GHz/mV). For higher bias voltage tuning a quadrating function would need to be used in order to fit to the function.

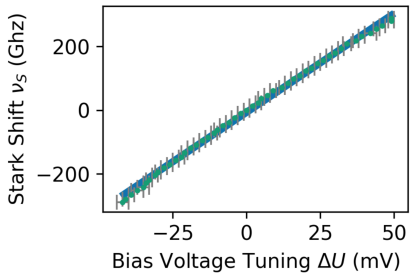

Figure 26: Dependence of the Stark shift on bias voltage tuning fitted using linear function [80]

Before the next measurements bandwidth of the grating filter setup which building scheme is shown on Fig. 19 was determined. The grating filter is an important part of the setup as it enables a laser filtering in order to filter out the excitation laser and use APD detectors which are highly sensitive. It can however limit the linewidth of the QD's emission due to finite bandwidth. To determine the bandwidth of the grating filter a tunable, cw DLPro laser was used. The grating filter was aligned for 797.3 nm which is in accordance to the highest emission intensity of a selected QD1 at 1.39V (investigated in the course of this thesis' project). The laser was tuned in the range of 797.1 to 797.4 nm and set for a stabilized power of 1 μW. Counts for each laser frequency were detected on the APD

detector (Fig. 27). Additional filtering of an absorptive ND (neutral- density filter) 10 was needed to not saturate the APD detector and remain in the linear detection regime.

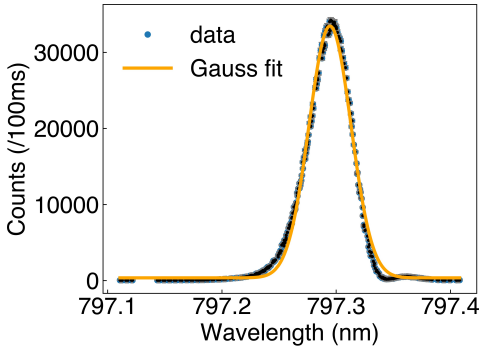

Figure 27: The bandwidth of the grating filter. Measured data fitted using a Gaussian function.

The dependence of the detected counts on the laser frequency was fitted using a Gaussian function. From the results a FWHM of 43.28 $\pm$ 0.26 pm was obtained which gave a bandwidth of 21.64 $\pm$ 0.13 GHz.

The efficiency of the grating is limited by the grating diffraction efficiency and additional optics in the setup. The reached efficiency of the setup is around 70% (laser power measured at the input and before collection fiber coupling- Fig. 18). The fiber coupling is around 50%.

6.2.1 *Time- resolved exciton state lifetime*

In the next steps the linewidth of the QD1 at XK was estimated. For this purpose the grating filter was aligned for the emission line from QD1 at 1.4V. Since the bandwidth of the grating filter is roughly 21.64 $\pm$ 0.13 GHz, the filtering setup needs to be precisely aligned for selected QD line. As the emission is tuning along with applied voltage, the alignment of the grating filter also needs to be changed for highest collection efficiency at desired bias voltage.

Time-resolved measurement revealing the exciton state of a QD1 lifetime was performed using tunable Ti:Saphire laser 73MHz rep rate, 5ps pulse width (Mira laser). The resolution of the measurement is determined by the laser's pulse width, which for the Mira laser is 8 ps, and by the time resolution of the detectors (Fig. 28). Two APD detectors were used during measurements which for 800 nm have an efficiency of around 60%.

The time resolution of both detectors is accordingly around 0.39 ns and 0.56 ns, which are much slower comparing to the laser's pulse width. An exciton lifetime measurement is important to investigate how the exciton state from which the photons are emitted is limited in time. The emission spectrum of an ideal two-level emitter has a linewidth limited by the radiative lifetime of the transition $\Gamma_0 = \frac{\gamma}{2\pi}$. The decay rate γ can be extracted by fitting the data to an exponential decay convolved with the instrument response function (IRF). IRF signal was obtained by measuring the laser signal through the transmission of the setup. The IRF signal on Fig. 29 consist of additional peak which is caused by multiple reflections of the signal before detecting using APD detector.

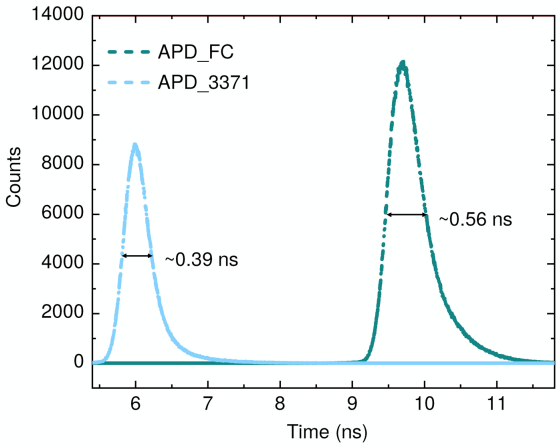

Figure 28: Time resolution of APD detectors used during the measurements. The time resolution of each detector was estimated by the FHWM of the peak of measured laser pulse.

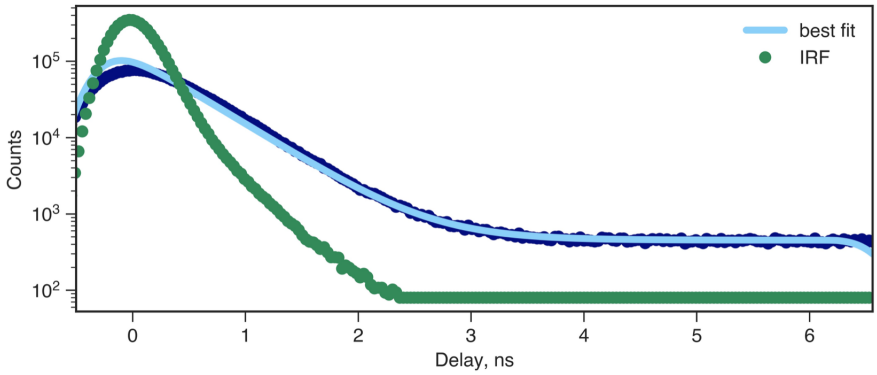

Figure 29: An exciton lifetime measurement of selected QD1 using Mira laser at XK. The blue line is a fit to an exponential convolved with the IRF (green).

The decay of the line enables to estimate the lifetime of an excitonic state. The fit on the data revealed the lifetime in the order of 460 ps. Thus it was possible to calculate the lifetime-limited linewidth to be $\Gamma = 347.6 \pm 2.8$ MHz. The linewidth of a QD is always limited by intrinsic broadening (natural broadening) which is directly related to the principle of Heisenberg. It relates the lifetime of an excited state (due to spontaneous radiative decay or the Auger process) with the uncertainty of its energy. A short lifetime of a QD will have a large energy uncertainty and a thus a broad emission.

For droplet QDs in a bulk material in [17] a 0.59 ± 0.01 GHz linewidth was measured, which corresponds to a lifetime of 1/T = 270 ± 3 ps. A Purcell effect of a QD integrated into the PhCW allows to shorten the lifetime of the emitter and thus an increased spontaneous emission rate is expected. However, comparing both results, the lifetime of an emitter did not increase in a PhCW. The exciton dynamics strongly depends on the LDOS at the position of the QD inside the PhCW [57]. Due to the fact that the spectral position of the QD is far away from the band-edge of the photonic crystal (expected band edge of 810-820nm) a weak Purcell factor can be expected. Previously the band-edge around 814 nm was measured for the sample with equivalent fabrication parameters (see Fig. 13b).

In the next measurement an emission from a QD1 as the function of applied gate voltage was measured using APD detectors. Before the detection a grating filter was aligned for a QD1 emission at 1.39V (which corresponds to 799.26 nm). An out-of-plane, quasi resonant excitation was used, which enables to determine the dependence of detected counts on bias voltage. The results are shown in the Fig. 30.

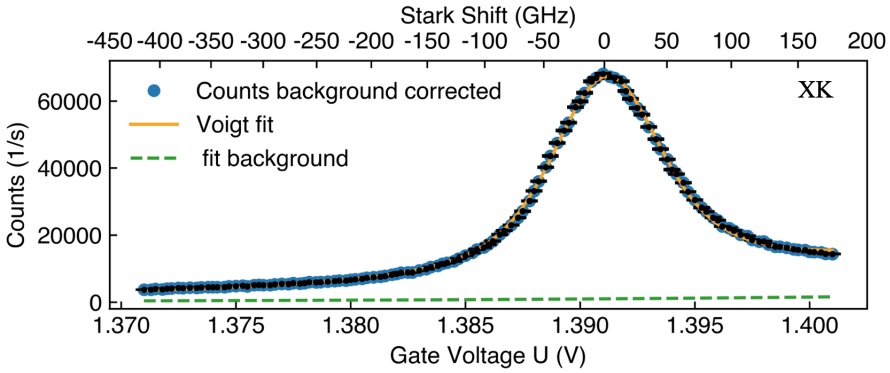

Figure 30: The dependence of detected counts from QD1 on applied voltage after grating filter setup. The single emitter was excited quasi-resonantly from the top at 784.91 nm and 15 μW.

The convolution of Lorenzian and Gaussian functions (Voigt) and a Gaussian function was used in order to perform the most accurate fit. The Gaussian function was set to be very close to the main peak with much lower amplitude. The main peak was fitted using the Voigt function. From the fit, using FWHM, the excitation linewidth of 5.969 $\pm$ 0.077 mV was determined. The quasi resonant excitation is accompanied by the phonon relaxation processes, which happens on tens ps timescale. The final spectra of a QD is the product of the width of the quasi resonant excitation (Fig. 30) and the grating filter profile (Fig. 27).

Using the estimated Stark Shift, as a gate-voltage to resonance frequency calibration it was possible to determine the width of the quasi excitation in GHz: 39.1 $\pm$ 1.4 GHz. The quasi resonant excitation linewidth involves phonon relaxation which gives wide linewidth of the p-shell transition. At higher temperature the phonon relaxation will be faster and therefore a broaden excitation line is expected [81, 82]. As the measurement was performed in high temperature XK (estimated between 15- 20K) the thermal broadening by phonons can be very large [83].

However, there are also other factor which are causing the broadening of the excitation/absorption line. The exciation line broadening also depends on the excitation method and power density (power broadening). If we reduce the influence of QD environment (use the excitation frequency which only excite single a QD) it will result in narrower emission spectrum. Using the resonant excitation the phonon relaxation processes that accompany quasi resonant excitation scheme are removed. This is because the quasi resonant excitation puts the QD into higher-order shells (p-shell, d-shell and so on). Such that further emission from s-shell that is detected is accompanied by the phonon relaxation. Hence expected decreased broadening for resonant excitation, which enable the study of intrinsic properties of a single QD.

6.2.2 *Resonance Fluorescence*

In this section we present the obtained resonance fluorescence spectra from selected QD1 embedded in a PhCW at XK.

To generate single photons from a QD, an out-of plane resonant excitation or an excitation though a waveguide modes is needed [84]. In order to efficiently excite QD in resonance the exact location of QD needs to be identified, such that the excitation laser can be focused on the QD from above. From the resonant excitation a resonance fluorescence (RF) is obtained. It is difficult to perform RF as it is difficult to filter spectrally the excitation laser. Since the collection of light generated by a QD is through the SEG couplers there is a spatial separation between the excitation and collection. However, the excitation laser is still making a lot of background and therefore a special laser filtering is required as well as high performance of all optical elements and a bright quantum source. To obtain RF a polarization optics was used on both excitation and collection path. The polarization optics (half-wave plate, quarter-wave plate and polarization filters) was used to cross polarize the excitation laser.

In order to find a resonant excitation frequency with the QD1 emission line the DLPro laser was carefully tuned with a fine steps. After finding a matching laser frequency the RF was measured having 1V as a background reference (Fig. 31).

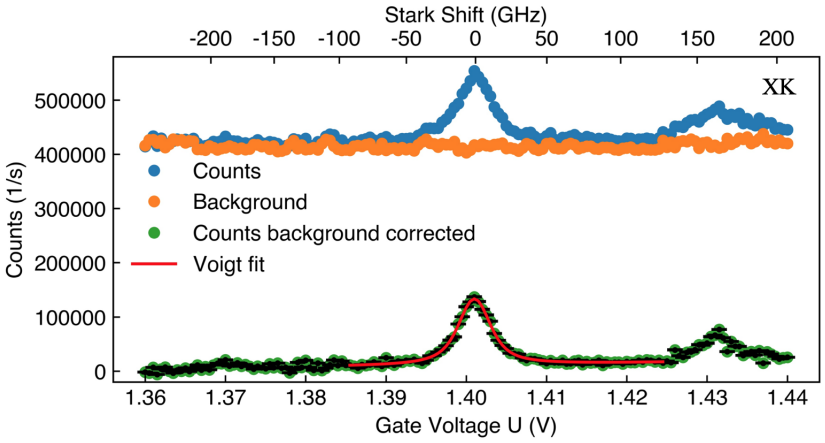

Figure 31: Resonance fluorescence of selected QD1 embedded in PhCW, performed under cw 100 μW excitation at 799.1 nm. Measurement performed at XK.

The RF was measured without grating filter. The excitation laser caused a lot of background counts and signal-to-noise ratio is therefore very low. The detected count rate was much higher (in the range of 130k counts/s) comparing to quasi-resonant excitation (around 60k counts/s) (Fig. 30) due to the higher efficiency of this excitation method. In order to receive the most accurate fit in Voigt function the Gaussian component was set to zero and therefore only Lorentzian component was taken into an account. The linewidth for resonant excitation is in the range of 28.4 $\pm$ 1.1 GHz. The smaller linewidth comparing to quasi resonant excitation is the effect of reduced phonon processes. The RF linewidth is limited by the spectral diffusion effects, while for quasi resonant excitation, the width is

mostly limited by the phonon processes. Additionally, for higher bias voltage a second peak can be seen which can corresponds to another charge state.

Quantum dot at 7K

As mentioned in the beginning of the chapter, all the measurements of QD1 embedded in PhCW were performed in two different temperatures. So far the results at XK (temperature between 15- 20K) were shown. In this section the results will be compared to the measurements performed at 7K. The temperature of the sample plays an important role since the energy band gap of semiconductor material is directly related to the temperature. As the temperature increases, the energy gap of semiconductor structures decreases, mainly due to the increase in the vibration amplitude of the lattice atoms and the bigger average distances between the atoms (lattice constant). The dependence of the energy gap E_g on temperature can be described phenomenologically using the Varshni relation [85]:

$$E_g(T) = E_g(0) - \frac{\alpha T^2}{T + \beta}, \tag{28}$$

where α and β are parameters of a given material. Changes of the energy band gap directly affect the spectral shift of emission wavelength from a QD. The p-shell (and other energy states) of a QD will accordingly change its energy. As mentioned before, lowering the temperature also reduce the interaction with phonons and therefore a narrower and brighter emission line is expected [86]. Analogously to previous measurements, the QD1 was firstly characterized in terms of applied bias voltage and its dependence on emission wavelength (Fig. 32).

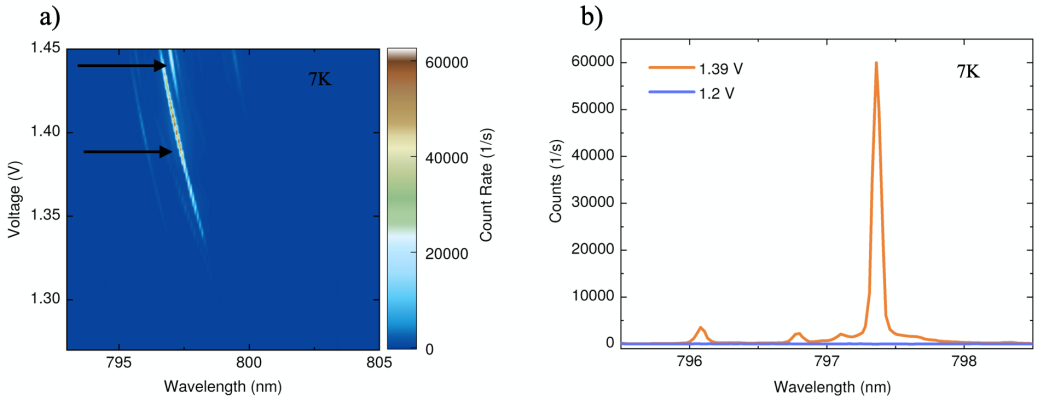

Figure 32: QD1 in PhCW excited quasi resonantly with 778.95 nm and power 50 μW. Measurement performed at 7K. a) Emission spectras measured at different applied voltages. b) the spectrum of the QD1 embedded in PhCW with applied voltage of 1.39V and 1.2V.

The first change that is clearly visible comparing to the measurement at XK (Fig. 25) is the „cleaner" spectra with much less lines which is caused by reduced charge noise. It is mainly reduced due to charges on the surface which in lower temperature are not disturbing the emission spectra as much. Again on the spectrum map a higher charge states can be distinguished and are marked with black

arrows. QD1 spectrum was compared for two different bias voltages. Fig. 32b shows a QD1 spectrum for quasi resonant excitation from the top for 1.39V and 1.2V. We can directly compare the spectrum with Fig. 25b, where analogous measurement was performed at higher temperature. At cryogenic temperature there are around 10 times more counts per second (for twice as little excitation power) and the spectrum has shifted by around 2 nm compared to XK. Moreover, the phonon sideband has significantly reduced. In order to compare the linewidth of the emission line, again a time-resolved measurement revealing an exciton lifetime of a QD1 was measured at 7K using Mira laser (Fig. 33).

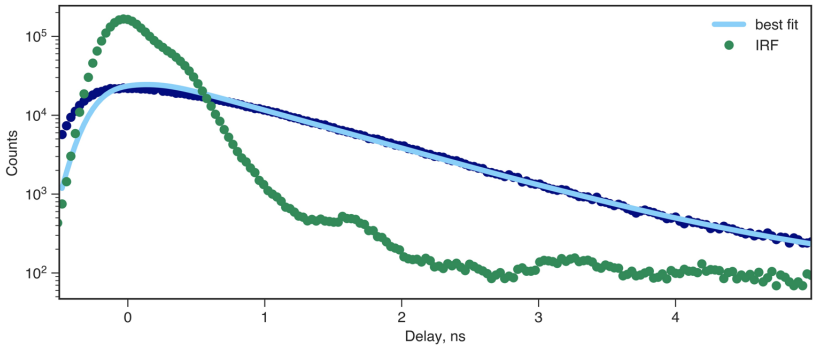

Figure 33: An exciton lifetime measurement of selected QD1 using Mira laser at 7K. The blue line is a fit to an exponential convolved with the IRF (green).

From the data fitting we extract the lifetime in the order of 904 ps. The lifetime-limited linewidth in 7K revealed to be equal to (174.1 $\pm$ 2.0) MHz, which is around 2 times smaller than the linewidth measured at XK. This might be caused by decreased phonon interaction at lower temperature. The mechanism of the temperature dependent exciton lifetime need to be further investigated

In order to directly compare the linewidth, the emission of a QD1 was measured as the function of applied bias voltage and detected after the grating filter on APD detector. The measurements were performed for both cw and pulsed excitation (Fig. 34).
For both measurements the Voigt function was used to fit the data. For pulsed excitation source, the width of quasi resonant excitation spectra at 7K is in the order of 25.56 GHz $\pm$ 0.91 GHz. For cw excitation the width of quasi resonant excitation spectra at 7K is 23.84 GHz $\pm$ 0.85 GHz. Both measurements were performed at different excitation powers, however, the width of the excitation spectra for both lasers remains similar. The linewidth has changed by around 16 GHz comparing to temperature XK. The linewidth change with temperature reported in the research conducted in [50] has revealed that the change of 16 GHz with regard to 7K corresponds to around 18K. In the mentioned paper, the investigated structure was based on InAs QDs embedded in GaAs photonic crystal waveguide. A similar measurement was performed for a selected QD1 (Fig. 35) [80]. The emission line of QD1 (excited quasi resonantly with constant power) at 1.39V was tuned from 7K to 35K and for each temperature the spectral position of the line was recorded. Despite different excitation methods with respect to [50] and a different QD material, both measurements revealed a similar dependence.

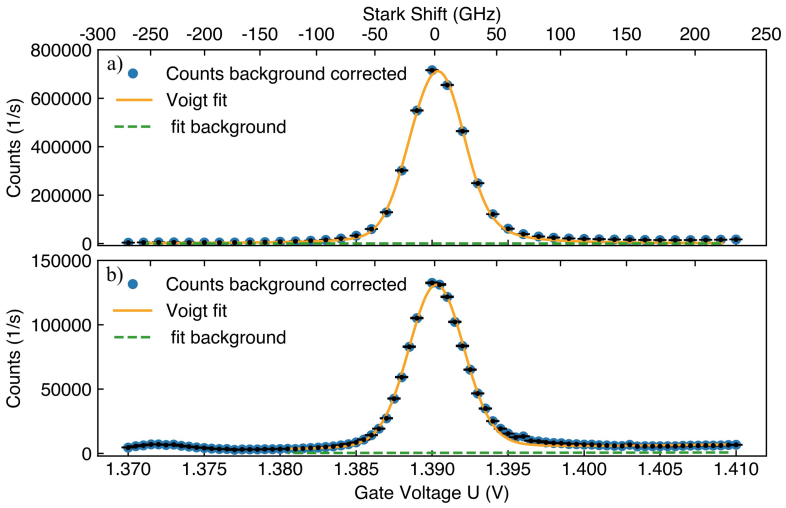

Figure 34: The dependence of detected counts from QD1 on applied voltage after grating filter setup excited quasi resonantly using a) cw laser at 778.92 nm and 50 μW. b) pulsed laser at 778.92 nm and 30 μW.

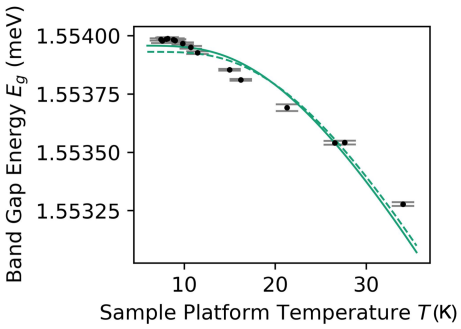

Figure 35: QD1 emission red shift with temperature [80].

In the next steps the dependence of the emission line on the excitation power is investigated in order to identify the exciton state from which the emission line origin.

The measurement was performed using quasi resonant excitation from the top, when the bias voltage was set to 1.39V. Fig. 36 presents a few QD1 emission spectras for different excitation power. For two highest excitation powers, the emission lines are limited due to the CCD camera saturation.

Next, the relative intensity of the emission line as the function of excitation power was determined (Fig. 37). The emission intensity at the maximum was determined by fitting the emission line with the Lorentzian function.

The measurements were carried out precisely enough to observe the saturation of the emission from the QD1 for the power of around 100 μW (Fig. 37). Saturation of the emission can be observed when the generation rate of carriers in the structure is equal or bigger than the rate of their recombination. Normally, for high excitation powers (for high carrier generation rates), the intensity of the emission decreases due to the occupation of higher energy states that must recombine in order to allow recombination into the ground state [87]. However, due to limited excitation laser power it was not possible to observe this phenomena in the investigated structures.

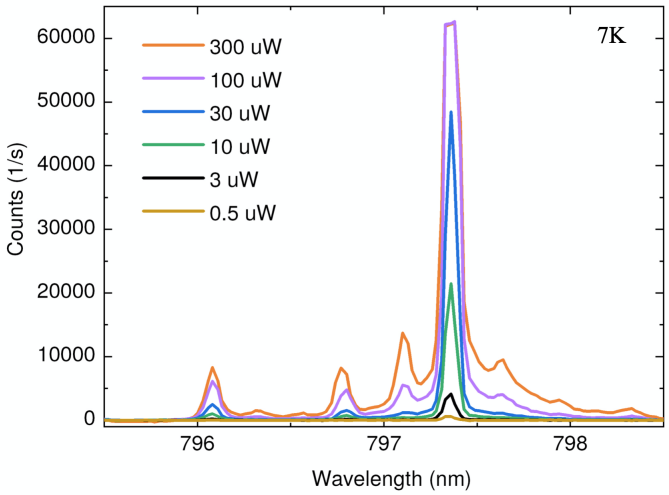

Figure 36: Quasi resonant spectra of a selected QD1 as a function of excitation power.

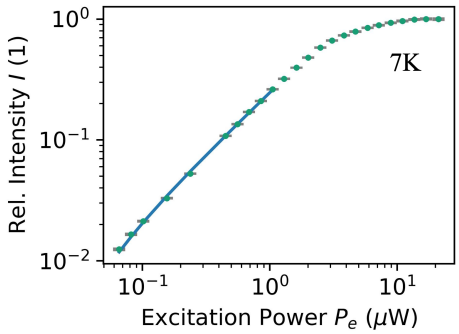

Figure 37: The relative intensity of emission line from QD1 dependence on excitation power.

The result data for low excitation powers were analyzed using the linear regression method with the slope of approximately 1 (Fig. 37). This allows to identify the emission line as an exciton (or a charged exciton - trion- see Sec.2.3). In order to unambiguously identify the emission line, the polarization properties of the emitted light should be investigated to determine its fine structure. When fine structure splitting in the zero field is too small (below the measurement resolution), it can be additionally increased by conducting the measurements in the magnetic field, but they were not carried out as part of the research for this thesis. Another way to to distinguish between exciton and trion is to study the radiative auger process [88].

6.2.3 *Single photon purity*

In order to characterize QD1 as a single photon source, its purity has been quantified by the measured degree of second-order correlation function $g^{(2)}(\tau)$. In this section we present the obtained results of measured $g^{(2)}(\tau)$ for both cw and pulsed excitation.

In order to have a low $g^{(2)}(0)$- high purity, the signal to noise ratio should be significantly high. Usually, it is most efficient using the resonant excitation, which reduces the interaction with the

environment of a QD and therefore decreases the background which is has to be much lower comparing to QD's emission line. Unfortunately, during the performed measurements the resonant excitation succeeded only for QD when the temperature was high (estimated 18K) and signal to noise ratio was too low to perform more advanced measurements. On the other hand, for the same QD at lower temperature (7K) the RF has failed (couldn't find the resonance of the laser and QD emission due to low signal to noise ratio). Therefore the second-order correlation function was measured using quasi resonant excitation, where signal to noise ratio was significantly higher (around 2500 for cw excitation and around 600 for pulsed excitation). Emission is collected and filtered on the grating filter and then using the HBT setup (Sec.2.5) the photons are correlated. On Fig. 38 a measured $g^{(2)}(\tau)$ function using quasi resonant excitation at 7K is shown.

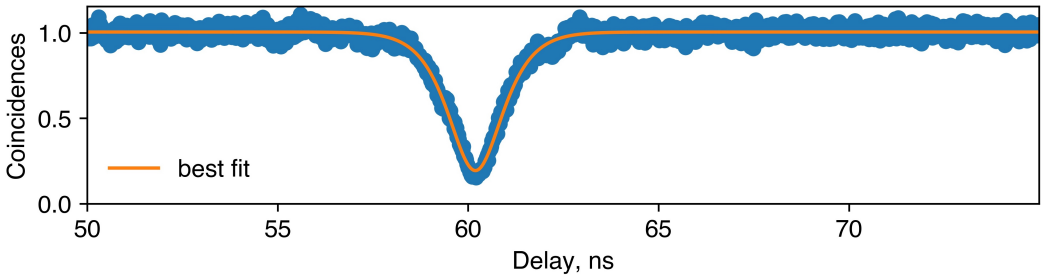

Figure 38: Measured second- order correlation function of the QD1 exciton using 30 μW cw, quasi resonant excitation at 7K.

Performed measurement revealed a $g^{(2)}(0)$ of 8.59% $\pm$ 0.82%. In order to calculate the a fit of the center dip is necessary. In order to fit the $g^{(2)}(\tau)$ function the instrument response function (IRF) needs to be taken into account. The IRF can be measured or it can be modeled using Gaussian function. The dip is a convolution between the IRF and a double sided exponential corresponding to the QD exciton lifetime. From the fit the linewidth of 186.7 $\pm$ 8.4 MHz has been measured, which is in accordance to the results obtained from the time- resolved spectroscopy (Fig. 33).

Same measurement was conducted using pulsed, quasi resonant excitation at 20 μW. Since it was difficult to find an ideal parameters value of a fit function, instead the area around $g^{(2)}(0)$ was integrated (Fig. 39). The single photon purity is quantified by the ratio:

$$g^{(2)}(0) = \frac{A(\tau = 0}{A(\tau \to \infty)}, \tag{29}$$

where A is the integrated area under the peak.
From the integrated area it was possible to calculate the $g^{(2)}(0)$ of 6.39% $\pm$ 0.91%. Performing $g^{(2)}(\tau)$ measurements leads to shorter lifetimes with respect to cw excitation [89].
The photon correlation measurements with pulsed excitation look different for cw. At $g^{(2)}(0)$ the peak goes to minimum as well as between laser pulses. The distance between coincidence peaks is determined by the repetition rate of the laser (for Tsunami laser the repetition rate is 12.5 ns).

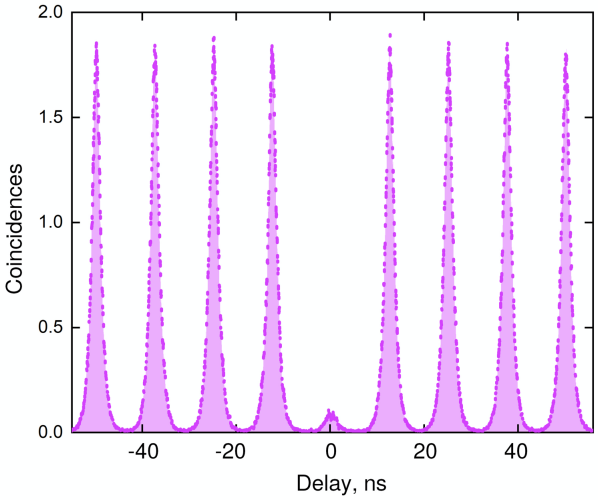

Figure 39: Quasi-resonant second order correlation function measured using pulsed excitation at 20 μW, data points integrated around 0 delay.

For characterized single QD1 embedded in a PhCW with a charge control the measured lifetime was longer than expected comparing to previous experiments due to spatial position of the emitter within the PhCW. The mechanism of the temperature dependent exciton lifetime need to be further investigated. The measured low $g^{(2)}(0)$ of around 6.4% proved that a single QD was investigated. Moreover, the $g^{(2)}(0)$ for cw excitation showed a similar lifetime in accordance with the $g^{(2)}(0)$ measured for pulsed excitation. The width of the RF spectra turned out to be much bigger than the natural linewidth, which could be both explained by the phonon dephasing (homogenous linewidth) and spectral diffusion (inhomogeneous broadening), the cause need to be further investigated. For measurements performed at 7K, where low contribution of phonon dephasing is expected, the line was 2 times more narrow comparing to estimated 18K. However, on the spectrum a charge noise is still visible which might be caused by the high current density through the n-i-p diode at the operating voltage of around 1.4V.

6.3 CONCLUSIONS AND OUTLOOK

Semiconductor QDs has been widely developed in the recent years as a potential deterministic, on-demand single photon sources for safe quantum communication application. Recent advancements in the fabrication of droplet GaAs QDs allowed for introducing a novel generation of QDs which show low-strain, long spin coherence properties, lifetime-limited linewidth which are not present for InGaAs QDs. The present work represents the first attempt on integration of GaAs QD into the nanophotonic structures compatible with an electrical control. The shorter wavelength gives challenge on nanofabrication as high resolution is needed to keep the high quality of the emitters.

As part of the thesis we studied an emission from a single GaAs QD embedded in a phonic crystal waveguide which show a great promise as a single photon source. The emission wavelength of the droplet GaAs QDs is compatible with rubidium based quantum memories which makes them a suitable candidates for quantum communication application. During the measurements we have characterized the nanophotonic platform as well as the optical properties of a single QD embedded within the PhCW. In the first part, the measurements were focused on the characterization of nanophotonic platform as well as the experimental setup. First, the impedance of a n-i-p diode, in which QDs were embedded, was measured which revealed the gate turn on at around 0.9V. The propagation losses of the waveguide were estimated in the range of 16.6 dB/mm. The high propagation losses are the factor that is still limiting the commercial application of integrated photonic circuits based on GaAs. Therefore an optimization of the fabrication process of nanostructures is a key for future realization of on-chip integrated quantum photonics including SPSs.

In the next steps a single QD in PhCW was characterized. The measurements were performed in two temperatures, first at XK (initially estimated between 15- 20K) and next in cryogenic 7K. For both temperatures the dependence of emission spectra on the applied bias voltage was determined. It enable to determine the Stark shift of 6.200 ± 0.045 (GHz/mV). By implementing a grating filter setup with determined bandwidth of 21.64 ± 0.13 GHz it was also possible to measure the exciton state lifetime of a QD embedded in a PhCW. The results were compared to the exciton lifetime of a GaAs QD measured in bulk in [17]. Since the exciton dynamics strongly depends on the LDOS at the position of the QD inside the PhCW [57] a decreased lifetime (which is related to an increased spontaneous emission of an emitter) was expected. However, due to the fact that the spectral position of the QD was far away from the band-edge of the photonic crystal a weak Purcell factor was observed. The measured lifetime were 2-3 time longer comparing with commonly observed in other experiments. This can be related to QD fabrication processes that need to be optimized in the future. The linewidth of the emission from QD in PhCW was also compared for both temperatures, where a decrease of around 2 times at lower temperatures was observed which is most probably caused be decreased phonon state interaction in cryogenic temperature. In the next steps the width of the quasi resonant excitation of 39.1 ± 1.4 GHz was determined at XK. The broader linewidth comparing to the grating filter was due to the quasi resonant excitation mechanism which involves phonon relaxation processes. The final spectra of a QD is the product of the width of the quasi resonant excitation and the grating filter profile. In order to reduce the linewidth broadening a resonance fluorescence measurement was

performed for QD embedded in PhCW at temperature XK. A significant reduction of the linewidth was recorded in the order of 28.4 $\pm$ 1.1 GHz, however very low signal to noise ratio made it impossible to continue with more advanced experiments. The broad RF line (100 times comparing with the lifetime limit) might be caused by the phonon broadening in the high temperature (measurement performed at XK initially estimated between 15- 20K), but also due to imperfect n-i-p diode which was operating at the high current density at 1.4V for high forward bias current of around 10 μA. Ideally the QDs should be measured for the bias voltage close to the gate turn on (for measured diode 0.9V) where the charge noise is reduced and therefore a decreased spectral diffusion is expected, however due to the low intensity of the QDs at voltages lower than 1.39- 1.4V it was impossible to perform further measurements. For quasi resonant excitation at 7K the same linewidth characterization was performed, where the linewidth of 23.84 GHz $\pm$ 0.85 GHz was measured.

The emission line of QD in PhCW was analyzed as function of temperature by [80]. By comparing it to the results in [50] it was possible to identify the temperature of XK as 18K, based on the difference in the linewidths for XK and 7K. The emission line was also measured as the function of excitation power. The linear behavior for low excitation powers enable to identify the emission line as an exciton.

After the basic characterization of the optical properties of the single QD in PhCW, a purity of the quantum emitter was investigated. The autocorrelation function $g^{(2)}(\tau)$ was measured using Hanbury Brown and Twiss configuration for both cw and pulsed excitation. Both measurement show $g^{(2)}(0)$ much bigger than 1, proving single QD excitation. Ideally to investigate the intrinsic properties of a single QD a resonance excitation is used which reduce the broadening of the line, however in our case it was impossible to find a resonance frequency of the excitation laser with the QD and therefore the $g^{(2)}(\tau)$ was measured using quasi resonant excitation. A single photon purity as low as 6.39% $\pm$ 0.91% was demonstrated.

This was a first attempt to characterize a novel droplet GaAs QDs embedded in photonic nanostructures compatible with electrical control. The measurements has proven that GaAs QDs embedded in PhCW are extremely bright and have a potential to reach significantly low $g^{(2)}(0)$. The factor that is still limiting the potential of these emitters are mainly the propagation losses in the waveguide. However, with improved fabrication technology processes and with very bright emitter there is a chance to obey this limitation. Since the selected QD was not ideally positioned in the band edge of the photonic crystal, a search for an emitter which frequency could overlap with the photonic band edge gives great promises regarding the enhanced spontaneous emission rate.

The purity of the source can be still enhanced by measuring it using resonance excitation. Moreover, for the full understanding of the emitters and their potential application as a SPSs the indistinguishability in Hong-Ou-Mandel experiment needs to measured as well.

BIBLIOGRAPHY

[1] H. J. Kimble, Nature, 453, 1023–1030 (2008)

[2] C. H. Bennett and G. Brassard, Theoretical Computer Science, 560, 175 (1984)

[3] P. G. Kwiat et al., Phys. Rev. Lett., 75, 4337–4341 (1995)

[4] Y. Yamamotot et al., Opt. Express, 20, 27510 (2012)

[5] X. He et al., Nat. Photonics, 11, 577 (2017)

[6] A. Kuhn et al., Phys. Rev. Lett., 89, 067901 (2002)

[7] A. Beveratos et al., Phys. Rev. Lett. 89, 187901 (2002)

[8] M. Gschrey et al., Nat. Commun., 6, 7662 (2015)

[9] X. Ding et al., Phys. Rev. Lett., 116, 020401 (2016)

[10] G. Juska et al., Nat. Photonics 7, 527–531 (2013)

[11] K. Hennessy et al., Nature, 445, 896–899 (2007)

[12] J. Gérard et al., Phys. Rev. Lett., 81, 1110–1113 (1998)

[13] N. Gisin et al., Nat. Photonics, 1, 165 (2007)

[14] P. Senellart et al., Nat. Nanotechnol., 12, 1026 (2017)

[15] W. W. Chow et al., Appl. Phys. Rev., 5, 041302 (2018)

[16] N. Tomm et al., Nat. Nanotechnol., 16, 399–403 (2021)

[17] L. Zhai et al., Nat. Commun., 11, 4745 (2020)

[18] H. G. Babin et al., Nanomaterials, 11, 2703 (2021)

[19] J. Wolters et al., Phys. Rev. Lett. 119, 060502 (2017)

[20] D. D. Sukachev et al., Phys. Rev. Lett. 119, 223602 (2017)

[21] J. Liu et al., Nat. Nanotechnol. 14, 586–593 (2019)

[22] P. Kultavewuti et al., Sci Rep 7, 5785 (2017)

[23] M. Gurioli et al., Nat. Mater., 18, 799–810 (2019)

[24] R. Uppu et al., Sci. Adv., 6, 50 (2020)

[25] P. Lodahl et al., Nature, 430, 654–657 (2004)

[26] T. Lund- Hansen et al., Phys. Rev. Lett., 101, 113903 (2008)

[27] M. Arcari et al., Phys. Rev. Lett. 113, 093603 (2014)

[28] K. Hennessy et al., Nature, 445, 896–899 (2007)

[29] R. G. Hunsperger, Integrated Optics: Theory and Technology, springer, 2009

[30] R. Uppu et al., Nat. Nanotech., 16, 1308–1317 (2021)

[31] J. Zultak et al., Nat. Commun., 11, 125 (2020)

[32] Q. H. Wang et al., Nat. Nanotech., 7, 699–712 (2012)

[33] M. A. Cotta, ACS Appl. Nano Mater., 3, 6, 4920–4924 (2020)

[34] W. A. Harrison, Electronic Structure and the Properites of Solids, Dover Publications, 1989

[35] J. Misiewicz et al., Optical Spectroscopy of Nanostructures, 2011.
[36] A. D. Yoffe, Adv. Phys., 42, 173 (1993)
[37] B. R. Nag, Physics of Quantum Well Devices, Springer, 2000
[38] A. Högele et al., Phys. Rev. Lett., 93, 17401 (2004)
[39] D. Haft et al., Physics E, 13, 165 (2002)
[40] A. Kiraz et al., Appl. Phys. Lett., 78, 3932 (2001)
[41] S. Seidl et al., Appl. Phys. Lett., 88, 203113 (2006)
[42] T. Mueller et al., npj 2D Materials and Applications., 2, 29 (2018)
[43] Y. Masumoto and T. Takagahara, Semicondutor Quantum Dots, Springer 2002
[44] L. Béguin et al., Phys. Rev. B, 97, 205304 (2018)
[45] E. Schöll et al., Nano Lett., 19, 2404–2410 (2019)
[46] M. C. Löbl et al., Phys. Rev. B, 96, 165440 (2017)
[47] J. Q. Grim et al., Nat. Mater., 18, 963–969 (2019)
[48] A. V. Kuhlmann et al., Nat. Commun., 6, 8204 (2014)
[49] R. B. Payel et al., Nat. Photon., 4, 632–635 (2010)
[50] H. Thyrrestrup et al., Nano Letters, American Chemical Society, 18, 1801 – 1806 (2018)
[51] Y. Arakawa et al., Appl. Phys. Rev. 7, 021309 (2020)
[52] H. Wang et al., Phys. Rev. Lett. 122, 113602 (2019)
[53] R. Hanbury Brown et al., Nature, 177, 27 (1956)
[54] L. Hanschke et al., Npj Quantum Inf. 4, 43 (2018)
[55] X. T. Zou et al., Phys. Rev. A, 41, 1 (1990)
[56] P. Michler et al., Science, 290, 2282–2285 (2000)
[57] P. Lodahl et al., Rev. Mod. Phys., 87, 347 (2015)
[58] F. Wen et al., Opt. Express 2008, 16, 16, 12278
[59] E. M. Purcell1, Phys. Rev., 69, 674 (1946)
[60] A. Glikin et al., Mater. Struct., 6, 155–158 (1999)
[61] E. Ruiz-Agudo et al., Chem. Geol., 383, 132–146 (2014)
[17] L. Zhai et al., Nat. Commun., 11, 4745 (2020)
[18] H. G. Babin et al., Nanomaterials, 11, 2703 (2021)
[62] P. Mooney et al., J. Appl. Phys. 67, R1–R26 (1990)
[63] G. Rius: Electron beam lithography for nanofabrication, Universitat Autonoma de Barcelona, Bellaterra 2008
[64] S. Adachi, „GaAs and Related Materials", World Scientific Publishing, 1994
[65] H. G. Babin et al., J. Cryst. Growth, 591, 126713 (2022)
[66] L. Ranasinghe et al., Nanomaterials, 11, 690 (2021)
[67] C. L. Dreeßen et al., Quantum Sci. Technol., 4, 015003 (2019)
[68] O. Gazzano et al., Nat. Commun., 4, 1425 (2013)
[69] L. Dusanowski et al., Opt. Express, 25, 31122-31129 (2017)
[70] A. V. Kuhlmann et al., Rev. Sci. Instrum., 84, 073905 (2013)
[71] A. N. Vamivakas et al., Nat. Phys., 5, 198 (2009)

[72] P. Ren et al., Nat. Commun., 13, 3982 (2022)
[73] E. Schöll et al., Phys. Rev. Lett., 125, 23 (2020)
[74] Y. Wang et al., Appl. Phys. Lett. 118, 131106 (2021)
[75] F. Pedersen, PhD thesis 2020, Deterministic Single and Multi-Photon Sources with Quantum dots in Planar Nanostructures
[76] J. Wang et al., Opt. Commun. 327, 49- 55 (2014)
[77] S. G. Johnson et al., Appl. Phys. B 81, 283–293 (2005)
[78] A. V. Kuhlmann et al., Nat. Phys. 9, 570–575 (2013)
[79] G. Kießlich et al., Phys. Rev. B, 68, 125331 (2003)
[80] N. V. Hauff, paper in preparation
[81] D. Gammon et al., Science, 273, 5271 (1996)
[82] M. Arzberger et al., Phys. Rev. B, 62, 16 (2000)
[83] E. V. Denning et al., Opt. Mater. Express 10, 222-239 (2020)
[84] R. Uppu et al., Nat. Commun., 11, 3782 (2020)
[85] Y. P. Varshni, Physica, 32, 149 (1967)
[86] T. Braun et al., AIP Advances, 4, 097128 (2014)
[87] P. Holewa et al., Phys. Rev. B, 101, 195304 (2020)
[88] M. C. Löbl et al., Nat. Nanotechnol., 15, 558–562 (2020)
[89] J. A. Smyder et al, PCCP, 16, 25723-25728 (2014)